UNIVERSITY OF CALIFORNIA

Los Angeles

3D Sensor for High Resolution Touch Panel Using Bootstrapped Oscillator-based Self-Capacitance Sensing

A thesis submitted in partial satisfaction

of the requirements for the degree Master of Science

in Electrical Engineering

by

Yan Zhang

2014

ABSTRACT OF THE THESIS

3D Sensor for High Resolution Touch Panel Using Bootstrapped Oscillator-based Self-Capacitance Sensing

by

Yan Zhang

Master of Science in Electrical Engineering

University of California, Los Angeles, 2014

Professor Mau-Chung Frank Chang, Chair

An oscillator-based self-capacitance sensing front end system is designed for the commercial grade projected capacitive touch panel. The self-capacitance architecture has potential in terms of 3D extended-range sensing in the vertical (Z) direction however planar resolution (X and Y directions) resolution had to be compromised if it were directly applied to the panel, which is designed for change-transfer based sensors. Incorporating the technique of bootstrapping to null the coupling capacitance between sensing channels, planar resolution can be restored and better Z direction range can be achieved. The design is realized in 65nm and has submitted to TSMC for fabrication.

The thesis of Yan Zhang is approved.

Sudhakar Pamarti

_____

Kung Yao

_____

Mau-Chung Frank Chang, Committee Chair

_____

University of California, Los Angeles

2014

Table of Contents

List of Figures

List of Tables

Acknowledgement

This work has been sponsored in part by grant from Wintek Corporation. The parts they supplied enabled the testing of the concept prototype and the technical discussion with their engineers helped me with a better understanding of touch panels.

My deepest gratitude goes to my advisor, Professor Mau-Chung Frank Chang. He is the inspiration and encouragement behind every inch of progress made on this project. Many obstacles were encounter since the date of concept prototype and Professor Chang has always told me to never give up because there is always a solution.

I am also very grateful to HSEL alumnus Li Du, who designed the concept prototype and has worked with me in this design. His experience helped me understand the design challenges and our detailed technical discussion usually led to solutions. During implementation, Li and I worked side-by-side with high efficiency. Without his help, it would have been impossible to have the entire front end taped out within a few months' time.

I would also like to thank PhD candidate Yilei Li and Dr. Adrian Tang for the technical discussion on the idea of bootstrapping. I thank Dr. Frank Hsiao for implementing the digital readout circuit for this project.

Finally, I would like to give special thanks to Dr. S. J. Lee, who relied on his industrial grade design and verification methodology to supervise this project. Full suite of simulations, pre and post-layout, were completed to show the health of the design under all conditions. I believe that the time spent on verification is well worth the seeming delay of the tape-out.

Chapter 1

Introduction

1.1 Motivation

It is said that the advent of iPhone has completely changed the way people interact with their cell phones. However, there would have been no revolution if not for the new and improved touch interface. These trendy gadgets evidently have rejuvenated the touch-screen business, both monetarily and technologically. Nowadays, we are surrounded by electronics that are covered in a piece of “glass”. Besides the omnipresent smartphones, global tablet PC shipment is projected to reach 455 million by 2017, according to display supply chain information provider NPD DisplaySearch. A total of 2.8 billion touch-screen panels will ship in 2016, up from 1.3 billion in 2012, based on a report from another provider IHS DisplayBank. Interestingly enough, as can be seen from the iPad tear-down (Fig 1.1), the piece of “glass”, where the touch sensor resides, is the second most costly component inside such systems, exceeding memory and processor. With uprising economics, there comes technology development. New and better touch screens are constantly being marketed, such as the “Super Sensitive Touch” panel on the Nokia Lumia 920 and the in-cell touch panel on the Apple iPhone 5. On the research front, many showcases of touch sensor development at this year’s ISSCC report progress towards systems with lower power, 3D gesture recognition, and sub-mm resolution [1][2][3].

As intuitive as touch interaction can be, physical contact comes with several drawbacks and can bring severe inconveniences. Projected capacitive sensing (PCS), the

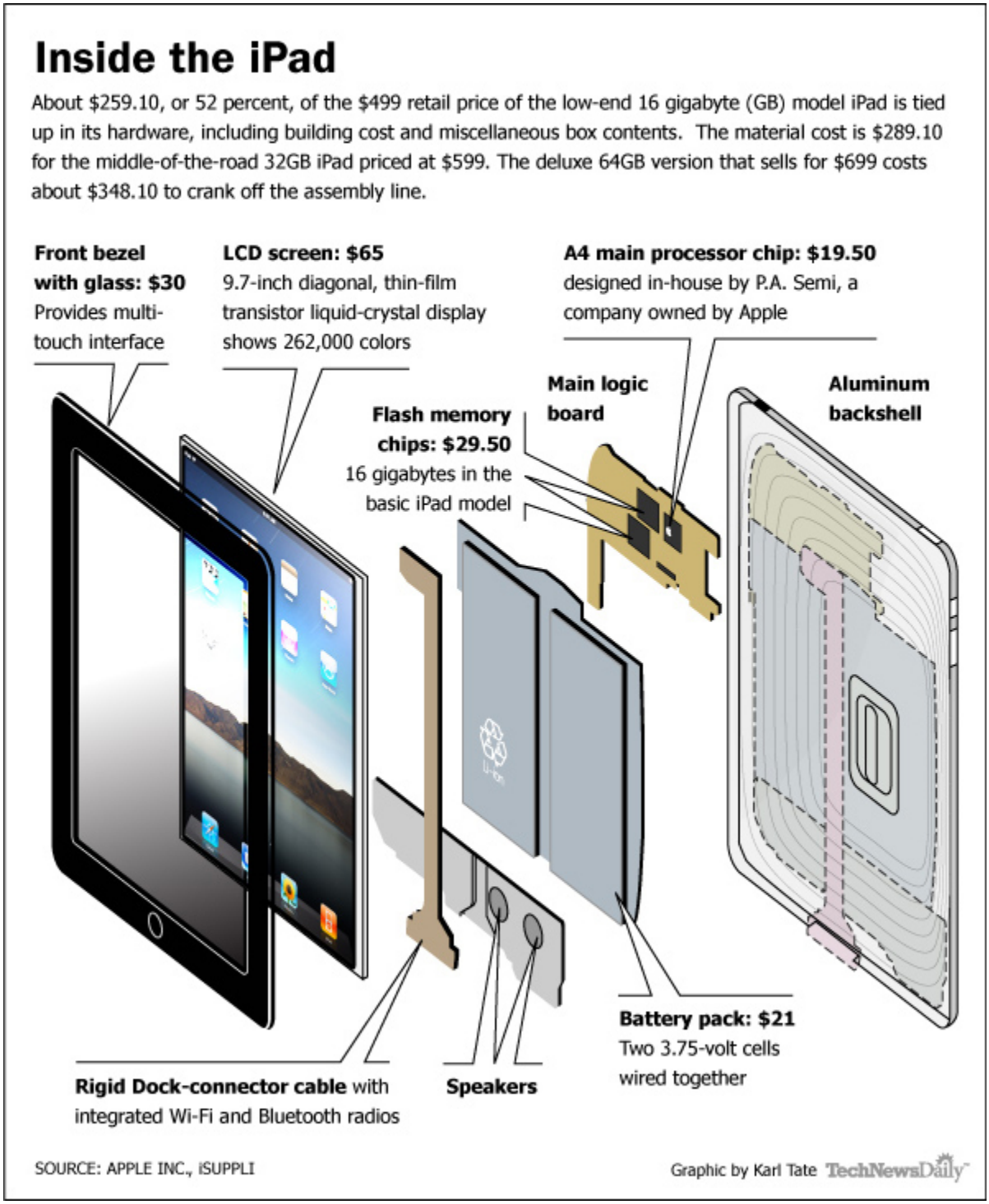

Figure 1.1 Teardown of an iPad

technology that are in about 80% of the touch screens, dictates a finger-only contact, prohibiting the use of gloves and other instruments as flesh-and-bone substitutes. Thus, in extreme and hazardous environments, choice of sensing technology is limited. In such scenarios, a sensing system that has a few centimeters to tens of centimeters range but with the same order of resolution is desirable. Such a high resolution contactless sensing system also alleviates hygiene concerns when the touch panel is used in a public setting, such as contact free authentication. Industrial design can also benefit because there will not be repeated pressure against the panel hinge or bezel, preventing mechanical breakdown and reducing bill of material. According to a new report "Gesture Recognition & Touch-Less Sensing Market by Technology (2D, 3D, Ultrasonic, IR, Capacitive), Product (Biometric, Sanitary Equipment), Application (Healthcare, Consumer Electronics, Automotive), Geography (Americas, EMEA & APAC) – Global Forecasts and Analysis to 2013 – 2020" by MarketsandMarkets, the total Gesture Recognition & Touch-less Sensing Market is expected to reach $22.04 Billion by 2020.

Among the choices of technology mentioned in the comprehensive report title above, 3D capacitive sensing can be designed to be completely compatible with existing PCS infrastructure, adding negligible manufacturing cost. Research effort has been put into designing 3D capacitive sensing systems to be used with existing PCS panels in the High Speed Electronics Laboratory (HSEL) at UCLA. During this pioneering course, success was made in demonstrating the concept of frequency modulation (FM)-based or oscillator-based capacitive sensing scheme yet difficulties were encountered when the concept prototype was applied to the commercial panel due to the non-idealities of the PCS infrastructure. This work hopes to address these difficulties using circuit techniques

as a milestone towards a complete system, hardware and software combined, for commercial use.

1.2 Major Work and Organization of Thesis

This work presents several important improvements over original concept prototype featured in Oscillator-Based Touch Sensor with Adaptive Resolution, a master's thesis by HSEL alumnus Li Du. The improvements target a few critical non-idealities when oscillator-based sensing scheme is applied to a PCS touch panel, which is designed for charge-transfer based sensors. The non-idealities were discovered and analyzed during an enduring process of debugging and characterization of the concept prototype. Circuit models were built to reflect these non-idealities and circuit solutions were first simulated and then prototyped with off-the-shelf components. In the end, a new integrated sensor front end was designed and taped out. Naturally, the organization of the thesis is:

Chapter 2 still gives a brief survey of popular sensing approaches with a major focus on PCS, since Li Du's has given an knowledgeable introduction to various sensing technologies in [4]. The understanding of PCS helps to comprehend the design of commercial panel. The potential caveats become clear when a different sensing approach is exerted upon it. Also, as PCS is the dominant technology today, its feature and performance dictate where the future work should go.

Chapter 3 explains the debug and characterization effort of the concept prototype and the touch panel. A complete lumped circuit model of the touch panel is presented. From the

model, the non-idealities become evident and the limitation of the concept prototype is justified.

Chapter 4 presents solutions to the problems revealed in Chapter 3, which include the application of bootstrapping and a redesign of oscillators. Various oscillator topologies are analyzed to justify the final design, which is based on an all-inverter active resonator topology.

Chapter 5 showcases the system level design of the integrated sensor front end where more improvements are inserted at the system level. Analysis of the impact of series resistance in the oscillator loading path to the sensitivity is also mentioned.

Chapter 6 concludes the work and gives a few ideas to polish in the future.

Chapter 2

Survey of Capacitive Sensing and Related Technologies

2.1 Overview

Touch sensing comes a long way – childhood memory of playing with stylus-equipped personal digital assistant (PDA) is still lingering. These early touch interfaces relied on resistive touch sensing, which was very popular during the past ten years and is still indispensable in low cost applications and where pressing action is preferred instead of touching. The concept of resistive sensing is quite simple: with a spacer layer sandwiched by two conductive layers, one of the layers is applied with a voltage gradient across one dimension; when the other conductive layer makes contact with it due to finger pressing, an intermediate voltage is measured and thus a proportional location along that dimension is calculated. Resistive sensing supports no multi-point touch and it gives user a slower and laborious feeling due to the pressing action. Even though capacitive sensing is definitely winning the market share, the fact that both resistive and capacitive uses glass panel with conductive coating, usually Indium Tin Oxide (ITO), and that both operates in the voltage/charge domain give them some similarities. For more information, [5] is a good resource which also contains introduction to infrared image based sensing and acoustic pulse recognition based touch sensor. Capacitive sensing techniques will be surveyed here as well as some introduction to ultrasonic based touch sensors, which can be a good contender in 3D sensing applications.

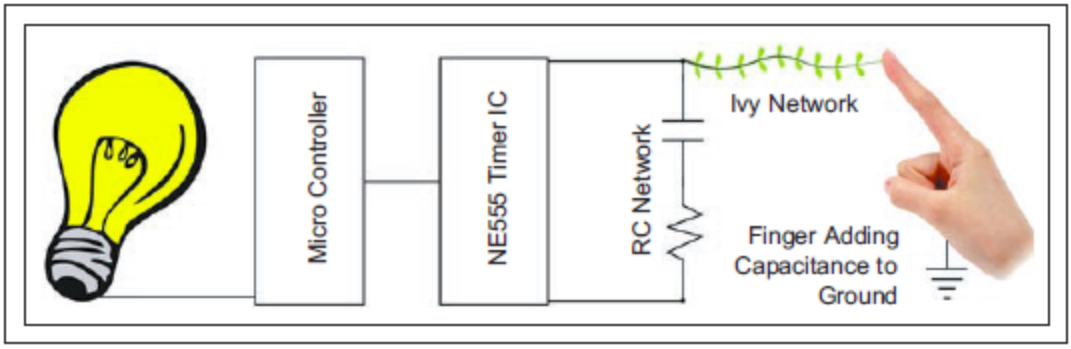

Figure 2.1 A capacitive sensing lamp based on RC time constant change

2.2 PCS – Self Capacitance

Although PCS is often publicly perceived as the new technology, the capacitance between our body (when grounded) and another conducting medium has long been utilized. Theremin, an early electronic musical instrument patented in 1928, works in a way that the performer's hand acts as the grounded plate (the performer's body being the connection to ground) of a variable capacitor in an L-C tank. This patent eventually leads to the inception of the concept prototype in HSEL. Another example, shown in Fig 2.1, is a 1970s-era capacitive-sensing lamp [7]. From the schematic, it is evident that the finger-added capacitance (finger cap, or C_F) changes the RC time constant that a timer IC (such as the NE555) relies on to generate timing signal. The microcontroller is programmed to detect the change and flip the switch. As rudimentary as these antique examples may seem, they are both part of the capacitive sensing family. Since in both examples the measurement is of the capacitance of a single electrode with respect to ground, they are called self-capacitance detection.

The working principle of self-capacitance is almost exclusive to monitoring frequency change, either L-C based or R-C based. Therefore the problem translates to

frequency change detection when a capacitance C changes to C + ΔC. One of the major obstacles lies in that C, which is the true self-capacitance from the sensing electrode to ground, is generally in the order of ten of pF whereas ΔC, the finger cap, is typically a few tenth of a pF or smaller. Directly coupling the C to an R or L leads to excessive use of controller time and power. In addition, the effect of noise is not mitigated in direct measurement. According to [8], a PCS system is mainly susceptible to three sources of noise,

1. Radiated noise, defined as noise radiated from circuitries surrounding the electrode, such as LCD, switching power supplies, RF components, etc.
2. Conducted noise, most commonly from noisy power supply and as well as the 50/60Hz AC coupling through human body.
3. Environmental changes due to fluctuating humidity, temperature, moving objects nearby and so on.

The most common technique to combat the above difficulties is to incorporate an integrating effect, such as using a sigma delta circuit shown in Fig 2.2. In this schematic, the sensor capacitance is continuously switched between two voltage levels using two non-overlapping clocks driving Switch 1 and Switch 2 respectively. The equivalent resistance of the switched capacitance, changing with C_F, modulates the duty cycle of the flip flop output. A timer is used again to measure the duty cycle for detection.

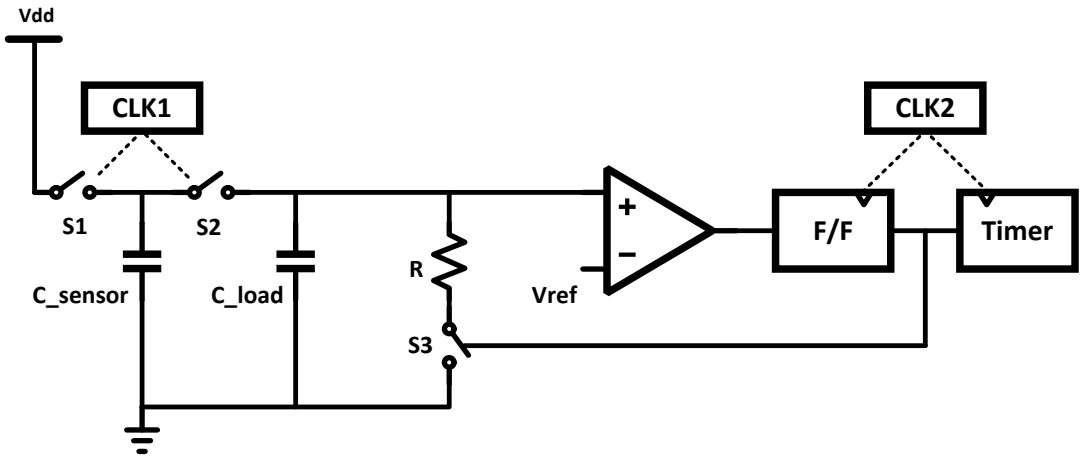

Figure 2.2 Sigma delta circuit for touch sensing

The approach illustrated above is based on the idea of a conventional relaxation oscillator. Even though sigma delta averages noise and duty cycle measurements circumvented long measuring time, the frequency drift of the oscillator due to environmental parameters and the uncertainly of digital delay renders the circuit less accurate. Another interesting idea involves the use of a relaxation oscillator [9] with feedback to stabilize the oscillation like that of a phase locked loop (Fig 2.3). Here the frequency of the VCO is set to be proportional to the RC network, which can be approximated as independent of process, voltage, and temperature variation as long as the external resistor is of high accuracy.

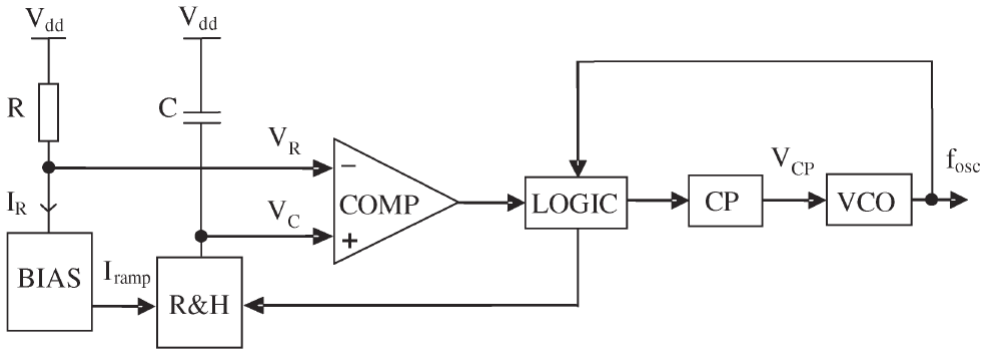

Figure 2.3 A relaxation oscillator with feedback for frequency stabilization

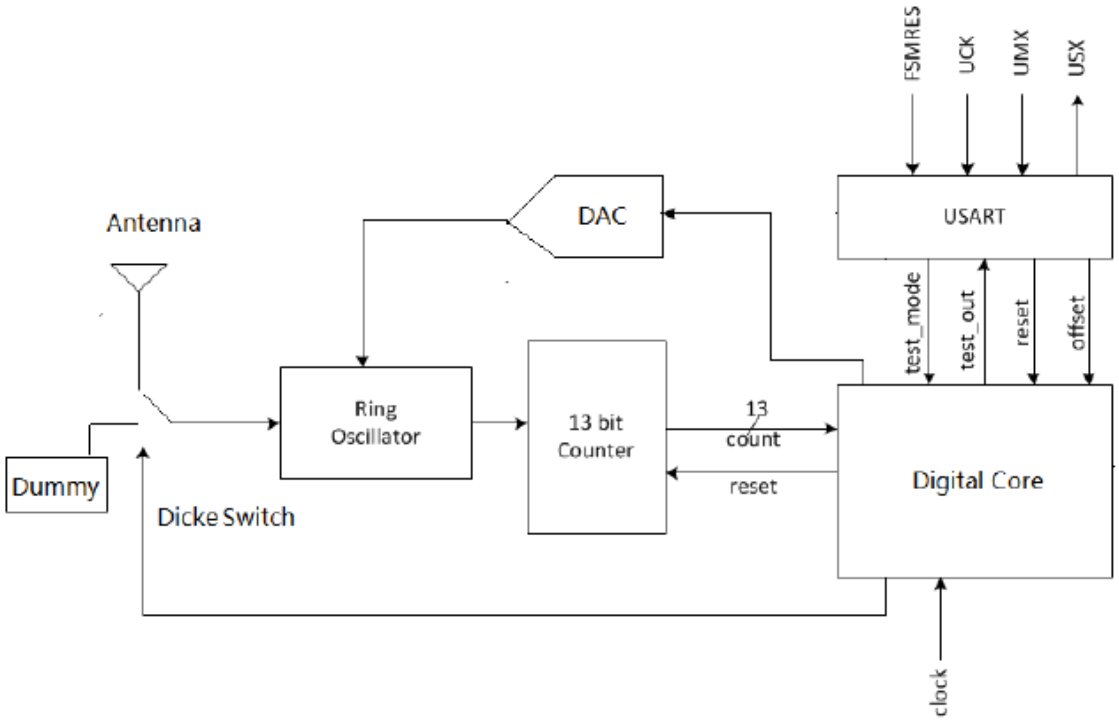

Figure 2.4 Block diagram of the concept prototype

The concept prototype developed in HSEL, shown in Fig 2.4, also adopted self-capacitance detection. The two major advantages of this architecture are:

1. The oscillator is designed to operate at much higher speed relative to the scanning rate of touch screen controller, which is typically around 200Hz. The effective number of cycles for (counter) integration is large enough to cancel high frequency noise.
2. The use of Dicke switches between a reference path and the C_F path cancels the effect of slow varying frequency perturbation such as oscillator frequency drift and that due to environmental changes.

Although this simple architecture is demonstrated in [4] for a single antenna (channel), many aspects remain to be perfected in order to apply it on touch panels designed for mutual capacitance detection.

2.3 PCS – Mutual Capacitance

In a self-capacitance touch screen, transparent conductive layers such as ITO are patterned into spatially separated electrodes in either a single layer or two layers. When the electrodes are in a single layer, each electrode represents a different touch coordinate channel and is connected individually to a controller. When the electrodes are in two layers, they are arranged in a layer of rows and a layer of columns. Each row and each column are again considered individual channels. By measuring each row and column one by one in a sequential manner, which is called scanning, the coordinates of the touch point is obtained. Mutual capacitance, on the other hand, measures the capacitance at the intersection of each row and column. This most prominent difference between self-capacitance and mutual capacitance dictates that at least two layers (rows and columns, X and Y, or TX and RX) must be constructed. Fig 2.5 illustrates the construction of a diamond patterned mutual cap panel.

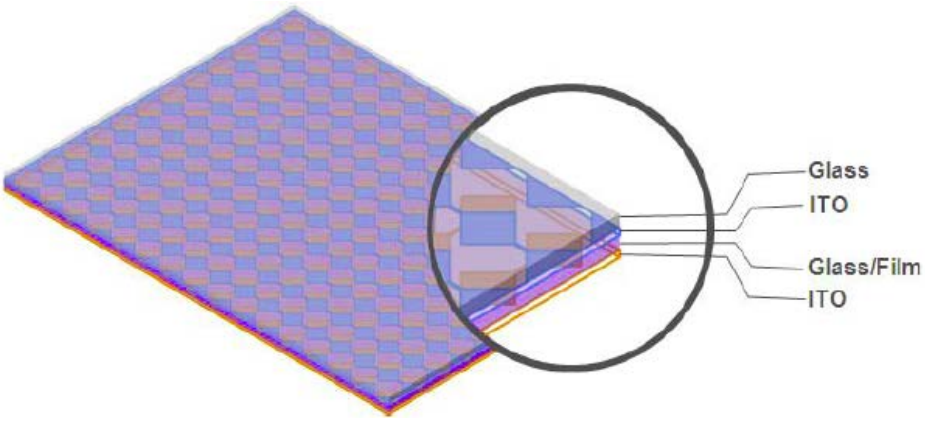

Figure 2.5 Physical construction of a mutual capacitance touch panel

With the capacitance stuck in the middle, the translation from passive elements to frequency or duty cycle is no longer straightforward. Thus, the detection strategy of mutual capacitance incorporates a capacitance-to-voltage conversion (CVC) process most commonly implemented by switched capacitor (SC) networks for charging the target capacitance [10]. The converted voltage is either fed into an ADC for digital processing or is discharged through a bleed resistor for discharging time measurement. More commonly CVC plus digitizing is combined in the form of a SC sigma delta modulator, shown in Fig 2.6. As shown, a known Vin repeatedly charges the unknown Cin and the total charge must be equal to the charge on Cref, which is charged by a Vref with digitally controlled polarization. The digital control word is the output as well. Since SDM offers excellent linearity and high resolution, the charge transfer based detection method ideally can detect changes in capacitance of a few fFs [11], which is sufficient for contactless sensing. In reality, this detection method has problems rejecting distributed noise such as LCD, RF and EMI interferences coupled to the electrodes. In addition, the non-idealities of the ITO electrodes, which will be covered extensively in

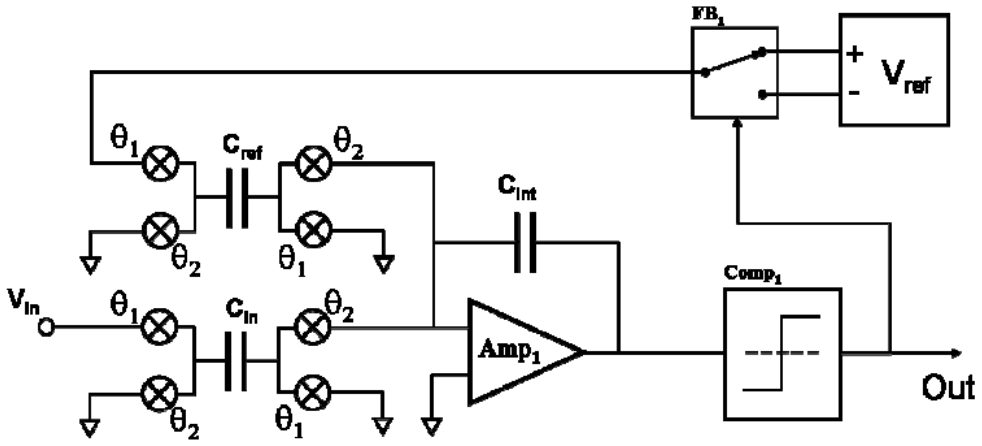

Figure 2.6 SC SDM for CVC with direct digital output

Chapter 3, limit full charge transfer and cause detection error. To avoid spurious detections caused by noise and environment changes, a signal-to-noise ratio (SNR) is defined for a particular system and the upper level firmware ensures that the SNR is met before detection is flagged. The definition of this SNR is an important performance metric for touch sensors and will be discussed later. Overall, charge transfer based detection approach is being perfected by designers on both system and circuit level each year with a few examples given in [3], [10], and [14].

2.4 Multi-point Touch Sensing (Multi-touch)

It is evident from the above discussion that mutual capacitance sensing requires more complex panel construction as well as more sophisticated interfacing circuitry, which add to both cost and power consumption. However, its unparalleled advantage to resistive or self-capacitance sensing is the capability to detect practically unlimited number of points at “the same time” whereas self-capacitance sensing can hardly sense two points. A run-down of scanning sequence of both detection methods illustrates this difference:

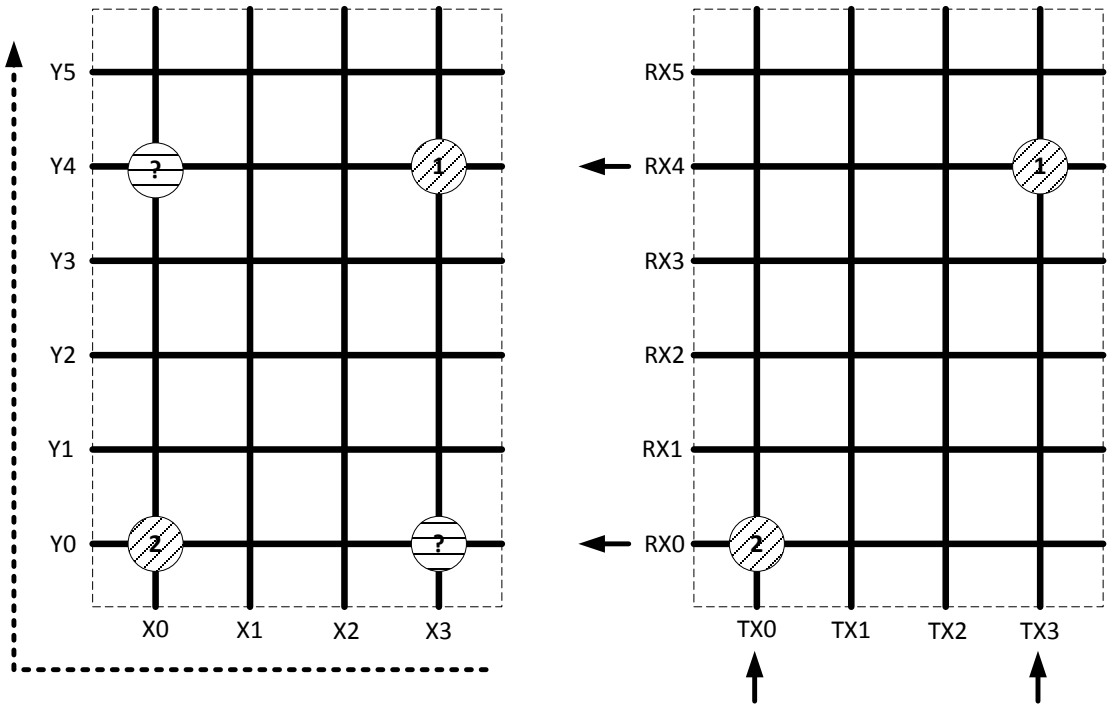

Figure 2.7.a (left) Scanning and location mechanism for self-capacitance sensing; 2.7.b (right) Scanning and location for mutual-capacitance sensing

1. In self-capacitance sensing, there is essentially no distinction of columns and rows. Each electrode is switched to the interfacing circuit one at a time until all electrodes are covered (no particular order is needed) and then one location reading is obtained. In Fig 2.7.a for example, the controller starts with electrode X3, moves to the left to X0 and Y0, and goes up to Y5. If a finger is present at (X3, Y4), the controller is expected to flag detection at the instant X3 is connected and also the instant Y4 is connected. However, if another finger is present at (X0, Y0), detection will be flagged for X0, X3, Y0, and Y4 – giving possibilities to a total of four points (X0, Y0), (X0, Y4), (X3, Y0), and (X3, Y4). Limitation of self-capacitance for multi-touch is therefore obvious and it is commonly termed “ghosting effect”.

2. In mutual capacitance sensing, since an active signal is injected to charge the capacitance at each row and column intersection, the rows and columns must be differentiated. The terminals into which the signal is injected are commonly referred to as TX; the terminal where converted signal is probed is RX. Scanning starts with the injection signal fixed at one TX (e.g. TX3) while all the RX's are probed sequentially (from RX0 to RX5), then the injection signal moves to the next TX (e.g. TX2), so on and so forth as shown in Fig 2.7.b. In this way, there is no ambiguity as each intersection represents a unique coordinate pair. Since the scan rate is faster than human's smallest perceived duration (100ms or so), the detection of multiple intersections appears to be simultaneous.

Even though it did not have much public exposure until Apple's work on the iPhone, the multi-touch implementation can be traced all the way back to the 1970s as a control room instrument at CERN for the Super Proton Synchrotron particle accelerator [13]. In my opinion, it is a truly ingenious design that has revolutionized human machine interface (HMI).

2.5 Sound-based Sensing Techniques

In addition to techniques in the electrical domain, sound-based detection approach offers a distinct advantage, which is the immunity to electrical noises. Various implementations exist and one that resembles PCS uses surface acoustic waves (SAW) arranged in a similar pattern as in a capacitive touch panel. Shown in Fig 2.8, two transmitting transducers output ultrasonic waves that overlay orthogonally through 90 degree reflectors over a glass panel. Since SAW get absorbed by soft materials such as

human skin, the presence of a finger on the glass panel blocks the transmission and the receiving transducer will detect absence of transmitting wave. SAW implementation is suitable for applications with touch screens of larger size, such as kiosk, arcade game, and automated machine interfaces. The main reasons are three folds: first, SAW can transmit long distance easily than dealing with huge parasitic capacitances if capacitive sensing were to be applied; second, SAW touch sensor does not detect a touch by hard materials which do not absorb pulse; and third, ultrasound transducers used to occupy substantial area which requires larger frame area for the screen. As technology such as MEMS advances, the dimension of ultrasonic transducers shrinks and starts to fit in power and area-limited applications. In addition, new ultrasonic techniques progress from planar detection to 3D ranging when radar-based configuration is used [2]. Ultrasonic imaging has had a long and glory history in medical field and it is undeniable that sound-based sensing has potential in human-machine interface.

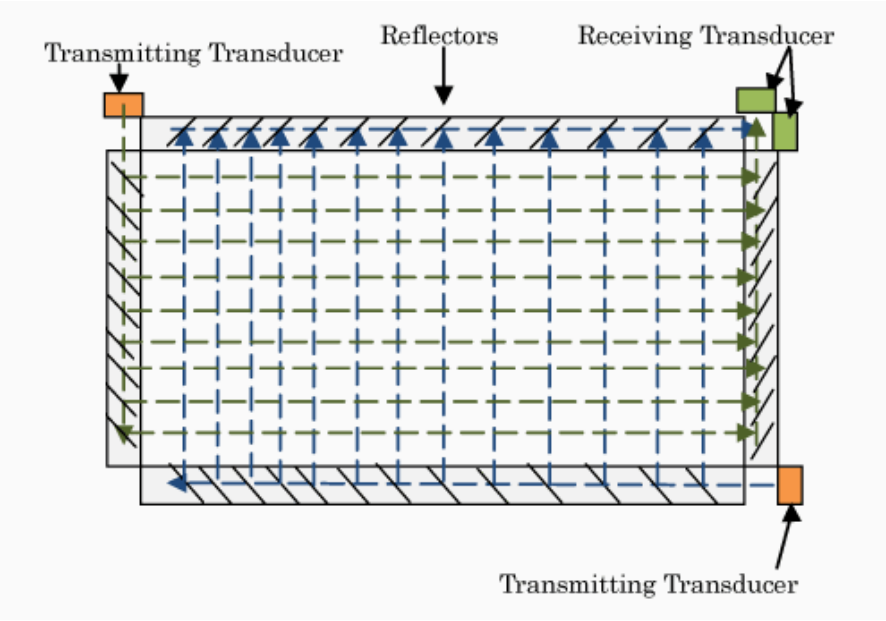

Figure 2.8 A SAW panel with properly located transducers and reflectors [5]

Chapter 3

Non-idealities of Panel Construction and their Impact on Sensing

3.1 Concept Prototype Test and Characterization

When the concept prototype featured in Fig 2.4 was fabricated and bonded onto a custom designed PCB, many questions left to be answered as for how the characterization process could be carried out to test the chip together with the PCS panel, and as well as to fully evaluate its 3D performance. The first difficulty encountered was that the digital read-out circuit in the concept prototype turned out broken, which prevented the assessment of the integrating effect of the high frequency oscillator and consequently. In [4], a digital oscilloscope was used as external frequency counter in order to demonstrate the change in frequency due to touch. Though laborious, frequency counter does give first order intuition of sensitivity and the overall noise can be cancelled to some degree by using built-in averaging function. This setup was used throughout the characterization of the prototype and panel. The second difficulty lay in that the adapter from the tightly pitched touch panel flex cable to the 0.1-inch-pitched solder board was not well manufactured. Through shorts-and-opens check, a few pairs of adjacent lines were found to be shorted and this caused some confusion mapping the panel hardware to the schematic, which was the only source for the connection between sensor locations and pin locations. The solution to this problem was to choose a few wires that, with no ambiguity (not affected by the shorts and opens), pointed to distinct locations on the panel. The design of an adaptor with solder pads turned out to be naïve because direct soldering (preferred in order to minimize path parasitic R and C) severely limited the re-

configurability of the test setup, as only one adapter was provided by our sponsor. Last but not the least, although literatures and application notes are full of design guidelines and test results for touch sensors, it was impossible to find a standard as in how the test were conducted and what apparatus was used, especially for 3D measurements. Holding a finger close to the panel was the rudimentary way used for testing the concept prototype, but that was only because there was no need for a better approach because the concept prototype did not perform well in the context of PCS panel. The concept prototype, which was designed for single electrode sensing, responded to finger touch as if the entire panel was one single electrode even though only one electrode out of fifty-two were connected. It was unable tell the location of touch even on a 2D basis.

3.2 Concept Prototype Debug and PCS Panel Modeling

It was perplexing at first as for how the change in capacitance on an unconnected electrode got coupled to the connected one, even when they were tens of cm's apart. Borrowing theory from CMOS substrate noise coupling, the suspicion that the coupling was through the glass substrate arose but it was quickly invalidated as the thickness of glass layer (on the order of millimeter) was much greater than the ITO layer (on the order of tenth of μm). Direct coupling from electrode to electrode was then considered. By using a precision digital multimeter, the capacitance between any two electrodes (simply referred to as coupling cap in this text, but not to be confused with Cc defined in the touch panel model below) on the 52-channel PCS panel was measured to be around 60pF. This coupling cap is potentially problematic as the effect of this coupling cap is illustrated in Fig 3.1.a and b.

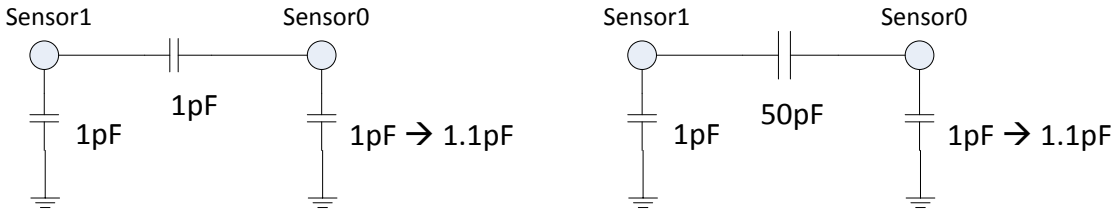

Figure 3.1.a (left) Two sensors with 1pF coupling;
b (right) two sensors with 50pF coupling

a. Effective capacitance seen at Sensor 0 is 1.6000pF and 1.5238pF at Sensor 1, a 4.8% difference.
b. Effective capacitance seen at Sensor 0 is 2.0804pF and 2.0703pF at Sensor 0, a merely 0.48% difference and at least decade of degradation in terms of achievable sensitivity.

Further examination of the PCS panel reveals the origin of the capacitance. A physical model [8] is shown in Fig 3.2 and a simplified lumped circuit model is shown in Fig 3.3.

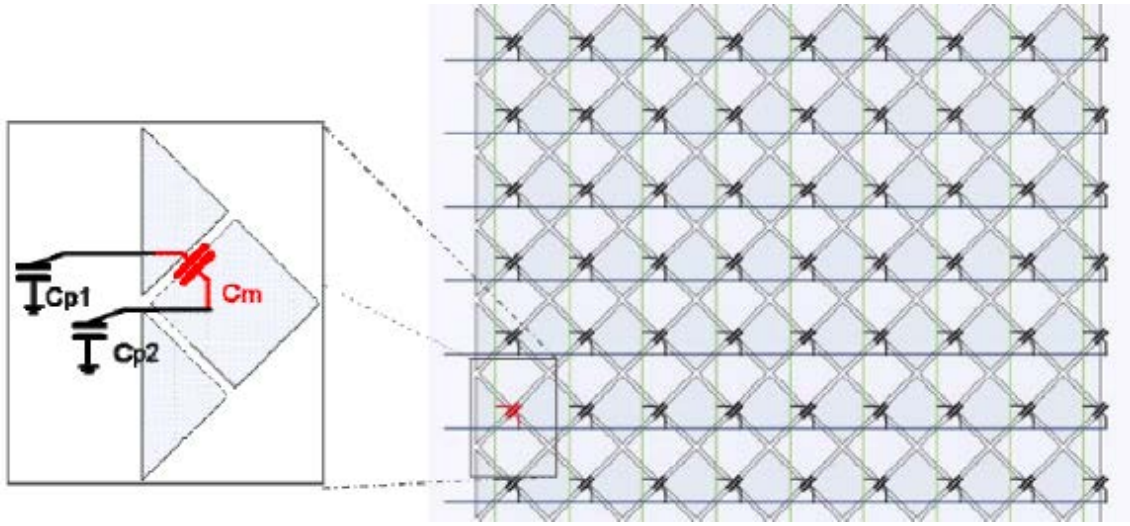

Figure 3.2 A diamond patterned panel zoomed in to show mutual capacitance, Cm

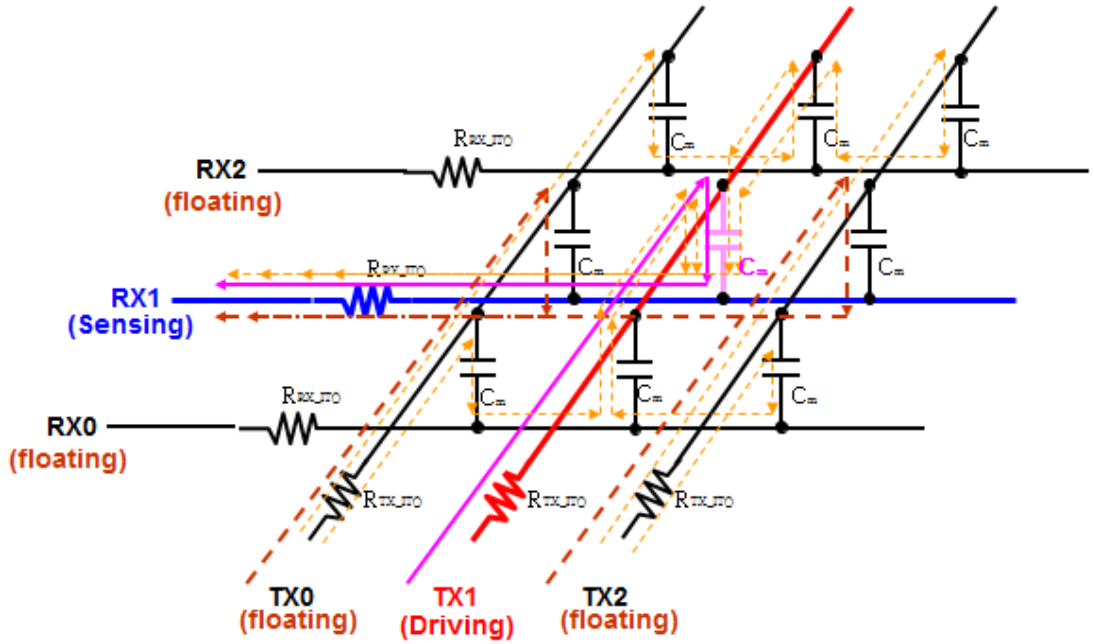

Figure 3.3.a Panel model with inactive channel floating, the configuration typical in self-capacitance sensing

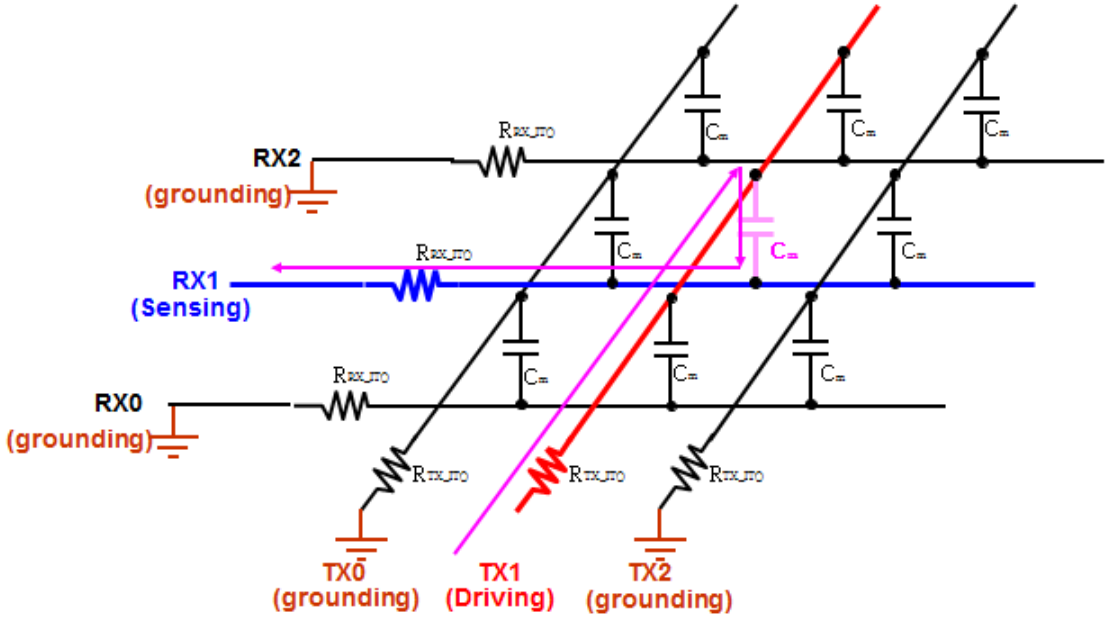

Figure 3.3.b the same model with inactive channel grounded, typical for mutual capacitance

The origin of the coupling cap is the mutual capacitance (Cm) at the intersection between TX and RX channels. One Cm may be less than 1pF according to literature. However, as can be seen in Fig 3.3.a, a matrix of Cm's exists in a parallel fashion between TX1 and

RX1 when all other TXs and RXs are floating. The dashed lines show all paths that have parallel capacitances due to Cm. In addition, the coupling between any two TXs and any two RXs (denoted Cc), further increases the total coupling cap. As a comparison, Fig 3.3.b shows the configuration during mutual capacitance sensing. Since an active signal is injected from one TX and is only sensed at one RX, all other TXs and RXs are grounded and all Cm's but one are effectively shorted. The coupling cap is a great challenge for applying oscillator-modulation based self-capacitance sensing to the same panel.

To complete the touch panel model, lab tests were conducted to measure all possible capacitances. For Cm measurement, all but one TX and all but one RX were grounded and the capacitance between the floating pair of TX and RX were directly measured. It was measured to be around 3pF including coupling along the wiring and adapter path (about 2pF). Cm inside the panel is considered to be within 1pF and 1.5pF in the complete model. The same direct measurement was used to get an estimate of Cc, which turned out to be comparable to the resolution of the multimeter and was set to be 1pF. In addition, each channel, TX or RX, has a self-capacitance to the infinite ground. The measurement of this capacitance was not straightforward. By using a signal generator and a capacitor network as illustrated in Fig 3.4, the self-capacitance, Cs, was measured to be around 5pF. A complete lumped circuit model of the touch panel is shown in Fig 3.5.

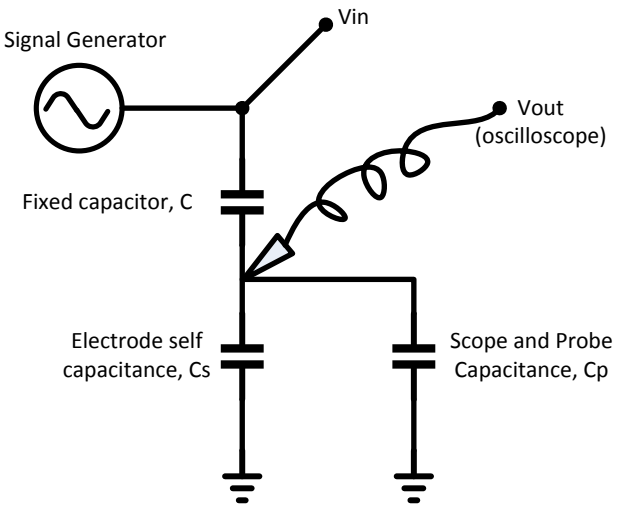

$$\frac{V_{out}}{V_{in}} = \left(\frac{1}{s(C_S + C_P)}\right) / \left(\frac{1}{s(C_S + C_P)} + \frac{1}{sC}\right)$$

$$\frac{V_{out}}{V_{in}} = \frac{C}{C + C_S + C_P}$$

Figure 3.4 The circuit configuration for measuring channel self-capacitance, Cs

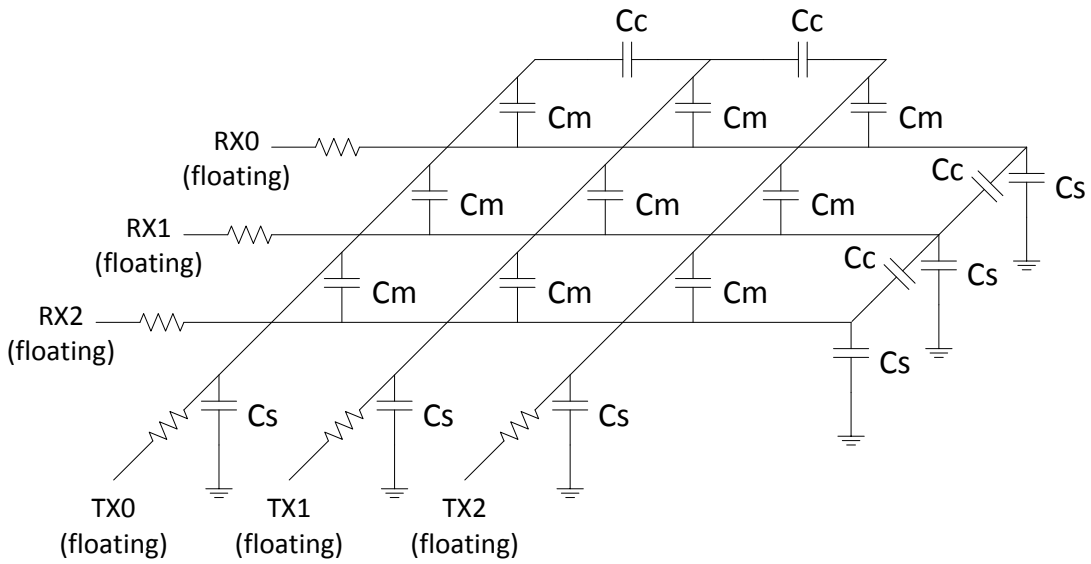

Figure 3.5 A complete lumped circuit model for PCS touch panel

3.3 Serial Resistance

Since the electrodes are made of conductive yet still resistive ITO traces, the serial resistance is an integral part of the model, as can be seen in Fig 3.3. In charge transfer based sensing, according to [11], the serial resistors are non-critical because they only slow down the settling process and some resistance is in fact deliberately introduced to improve electromagnetic interference (EMI) and ESD behavior. However, because the traces are of difference length and so are the serial resistance, detection error can occur in the capacitance-to-voltage conversion [14]. In the application of oscillator-based self-capacitance detection, the serial resistance was found to affect the oscillator output frequency and was also a key factor in determining the isolation, which was defined as the sensitivity of the sensor to capacitance change on non-connected electrodes. Since the on/off resistance of the switch contributes to this serial resistance, care was taken in designing the channel switches. The effect of the serial resistance will be mentioned again in system level design.

Chapter 4

Techniques for Nulling the Coupling Capacitance and Related Circuit Design

4.1 Bootstrapping

Having exposed the root cause of the negative impact of PCS panel on oscillator-based self-capacitance sensing, it is obvious that the best strategy to improve the concept prototype is to nullify the coupling cap. Referring to Fig 3.1, even though shorting the two sensors is the naïve and incorrect way to make the coupling cap go away, some hints can be drawn – if the voltage across the coupling cap is nulled, i.e. forced to be zero, then the effective coupling cap is non-existent. The two sides of the coupling cap can be connected to a voltage buffer to enforce equal voltages. Such a technique, with its origin in nullifying the effect of the input capacitance of a coax cable in front of a preamplifier (Fig 4.1), is called bootstrapping. The capacitance that is nulled is often said to be "bootstrapped out" [15].

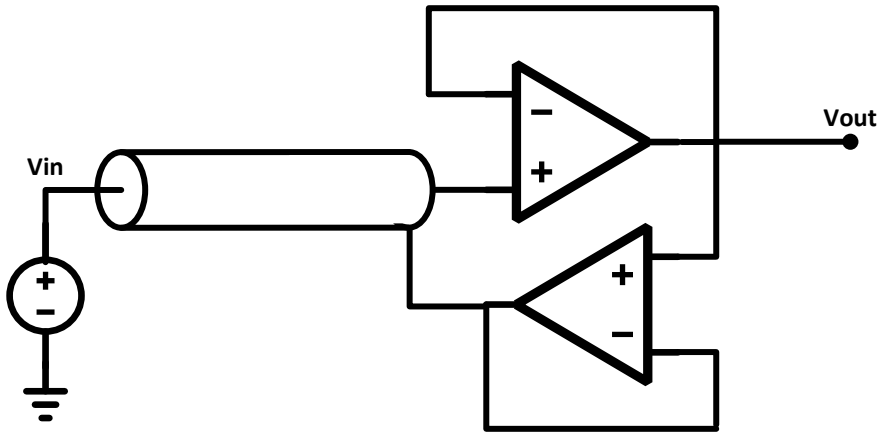

Figure 4.1 Bootstrapping for low input capacitance

Before diving into circuit details, the effectiveness of bootstrapping was first verified within the context of panel capacitor network in simulation. An ideal voltage-control-voltage-source configured as a unity gain buffer was used as the voltage buffer; an equivalent circuit of a diamond patterned panel with 14 TX's and 24 RX's was built into a RC network based on the model in Fig 3.5. Using ideal oscillator to estimate effective load capacitance of a single electrode (TX or RX), Table 4.1 is obtained. It can be seen that with bootstrapping, the total capacitance loading the oscillator is no longer dependent of coupling capacitors such as Cm and Cc and therefore only self-capacitance is measured. Since a voltage buffer requires only one op-amp and the whole setup can be added to the concept prototype easily with perfboard, an off-the-shelf op-amp, AD8031, was purchased and configured as a unity gain buffer for hardware verification of bootstrapping. Since the AD8031 has a unity gain bandwidth of 80MHz, the concept prototype was set to oscillate at a few of MHz to give the op-amp enough open loop gain. With bootstrapping added, two phenomena were observed: the oscillation frequency went up due to smaller effective load capacitance; the concept prototype was able to differentiate the connected electrodes from the non-connected ones based on the observation that the frequency change was discernable for touch on the connected electrodes but not on the non-connected ones.

TX-RX mutual capacitor Cm	3pF	10pF	10pF	10pF
TX-TX/RX-RX capacitor Cc	1pF	1pF	5pF	5pF
Self-capacitance to ground Cs	500fF	500fF	500fF	5pF
Total load without bootstrapping	14.5pF	20pF	20pF	>100pF
Total load with bootstrapping	510fF	510fF	510fF	5.3pF

Table 4.1 Simulation results indicating the effectiveness of bootstrapping

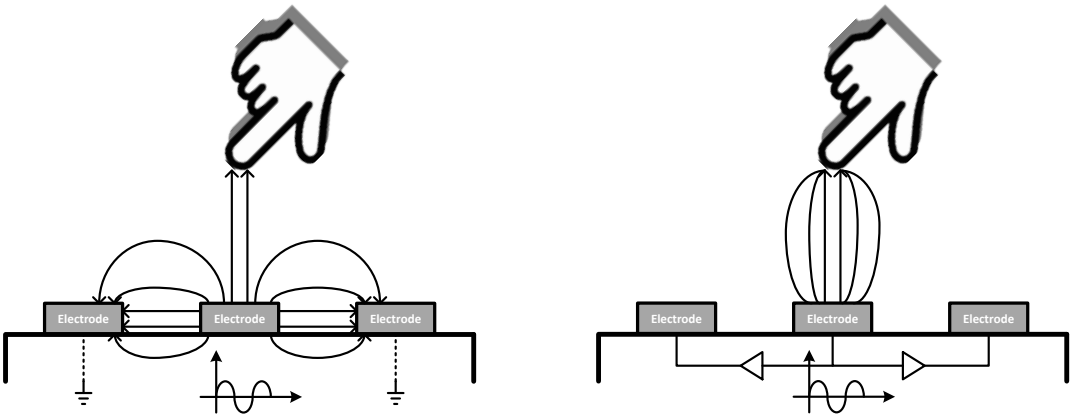

Figure 4.2.a (left) Electrical field line distribution without bootstrapping;
b (right) with bootstrapping

Besides the panel-wide coupling cap cancellation, bootstrapping can also increase sensitivity from the local touch interface. As will be mentioned in the system level design, bootstrapping is applied among all electrodes, which means they are forced to be at the same voltage at any given moment. Fig 4.2.a and b illustrates the change in the electric field lines with and without bootstrapping. Since the electrodes are equal potential with bootstrapping, the field lines from the measured electrode have to terminate all at the finger. In this way, the fringing lines are minimized while C_F is boosted.

4.2 Bootstrap Circuit Implementations

Voltage buffers are straightforward in terms of circuit design. Two flavors were considered, source-follower based voltage buffer and op-amp based unity gain buffer. In terms of circuit complexity and power consumption, a source follower has the obvious upper hand. However, with smaller technology node, the small signal gain of a source follower is getting further and further away from the optimistic unity. More importantly, in the presence of large load cap, the gain of a source follower diminishes even more quickly. Fig 4.3 shows the schematic within the context of a simplified capacitor network.

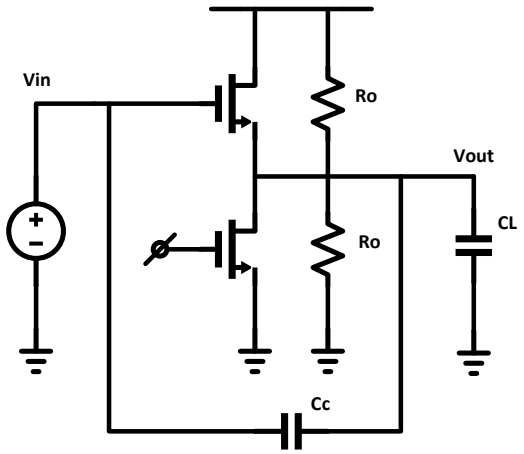

$$g_m(V_{in} - V_{out}) = G_0 V_{out} + G_0 V_{out} + sC_L V_{out} + sC_C(V_{out} - V_{in})$$

$$\frac{V_{out}}{V_{in}} = \frac{g_m + sC_C}{g_m + 2G_0 + s(C_C + C_L)}$$

At 5MHz, using typical values for short channel devices,

$g_m = 1mS$

$R_0 = 10k\Omega$

$C_C = 100\,pF$

$C_L = 100\,pF$

$$\frac{V_{out}}{V_{in}} = 0.6$$

Figure 4.3 Schematic of a source follower with coupling capacitor and gain calculation

Even with its gain disadvantages, source followers are still used for bootstrapping in [16], a 2014 ISSCC presentation on extended-range capacitive sensing using a similar approach as implemented here. In this competing work, an additional ITO layer is deposited beneath the layer of sensing electrodes and it serves as a reference plane for bootstrapping. Only 8 electrodes are used as the target application is different. Since the source follower connects the eight electrodes and the reference plan, it only needs to cover a much smaller coupling and load capacitance. The price is the increased manufacturing cost due to additional ITO layer and a 19mW overhead to drive the reference plane. Since the possibility to operate at much higher frequency is an important perspective to this work, the op-amp based unity gain buffer became the choice of design.

A simple derivation of the effective capacitance after bootstrapping with the unity gain buffer is shown alongside the schematic in Fig 4.4. It shows that high gain at the oscillation frequency is important in minimizing the difference between Vout and Vin.

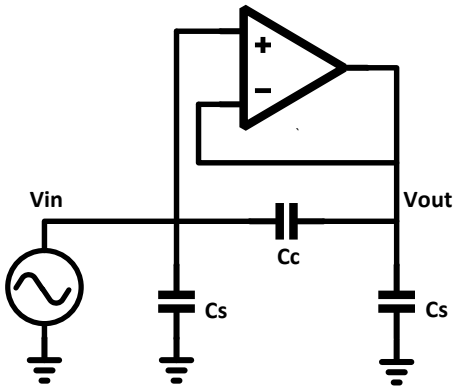

$$V_{out} = \frac{A}{A+1} V_{in}$$

$$C_{eff} = C_S + \frac{1}{A+1} C_C$$

Figure 4.4 Schematic of bootstrapping amplifier and effective capacitance derivation

The unity gain buffer essentially sees a capacitive load contributed by the self-capacitance of an electrode to ground, Cs (there would be some path resistances including the on resistance of the switches). Ideally, an op-amp with low output resistance should be designed to drive the combination of resistive and capacitive load with enough speed. However, due to the time constraint and the earnest consideration for simplicity and robustness, a simple two stage OTA with compensation and resistive zero-nulling was implemented for bootstrapping. With compensation and a load of around 5pF (Cs), the OTA was designed to have around 800MHz of unity gain bandwidth with 20pF of load. Since the coupling cap, Cc, is on the order of 100pF, a gain of 40dB is specified to reduce the effective Cc to be on the order of 1pF. More design detials and performance report for the OTA is provided in Chapter 5.

4.3 Bootstrapping Compatible Oscillator Design

With little math, a gain of 40dB can only be maintained for the OTA to 20MHz, a bound for all frequency components of the oscillation signal. If a ring oscillator with saturated waveforms is running at 10MHz, its harmonics will easily exceed 20MHz,

making bootstrapping less effective. For this reason, a sinusoidal oscillator is desirable. In addition, during the testing of the concept prototype, in which a differential ring oscillator was designed, it was very inconvenient to always have to balance the two loads for an acceptable duty cycle. Since the electrodes are single-ended load, it was decided to bring forward single-ended oscillator designs.

As a baseline for sinusoidal oscillator design, conventional LC tank oscillator has a simple topology with good stability and the possibility to achieve high purity. The differential nature of the cross-coupled pair makes it less desirable yet the more severe problem is the size of inductor for an oscillation frequency that is in the MHz range. Using the simple $f = 1/2\pi\sqrt{LC}$ relationship with C = Cs = 5pF and f = 10MHz, L is calculated to be 50uH. At this size, the inductor must be added as an off-chip component and it may be a undesirable feature as the internal space of a tablet or cellphone is very limited. Nonetheless, off-chip inductor gives a very high Q tank at this frequency range and it is used in [16].

Another variation of LC oscillator that can give good phase noise performance is the Colpitts oscillator [17], shown in Fig 4.5.a. Its inherent single-ended operation was so attractive that it was almost decided to use an external inductor as part of the design. Unlike the Class-A operation of the LC tank oscillator, the Colpitts oscillator is Class-C action. However, as can be seen from the derived equivalent circuit in Fig 4.5.b, the equivalent capacitance for the LC tank is the series combination of the two capacitors. For oscillator based sensing, the dependence of frequency on Cs should be as high as possible. For charge transfer based approach, the converted voltage is linearly dependent on Cs; for the conventional LC tank oscillation, the frequency is only proportional to

$1/\sqrt{C}$; and unfortunately for the Colpitts, the series combination of capacitors makes Cs even more irrelevant unless C_1 is unpractically large, mandating another off-chip component.

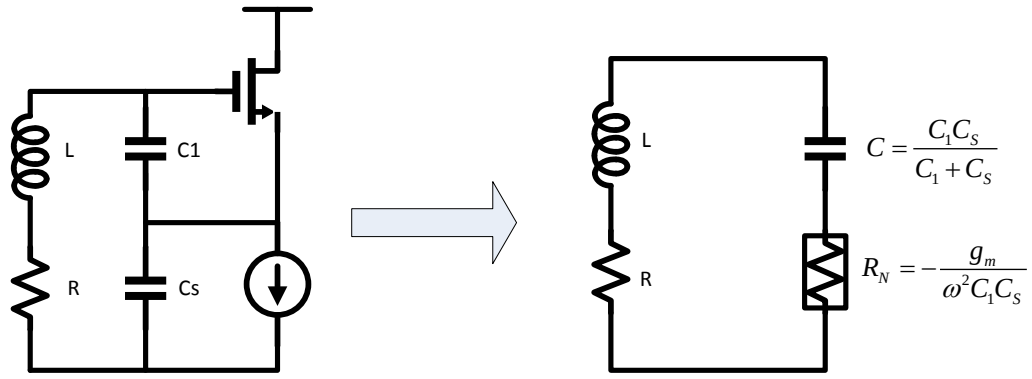

(a) (b)

Figure 4.5 Colpitts oscillator and its equivalent circuit

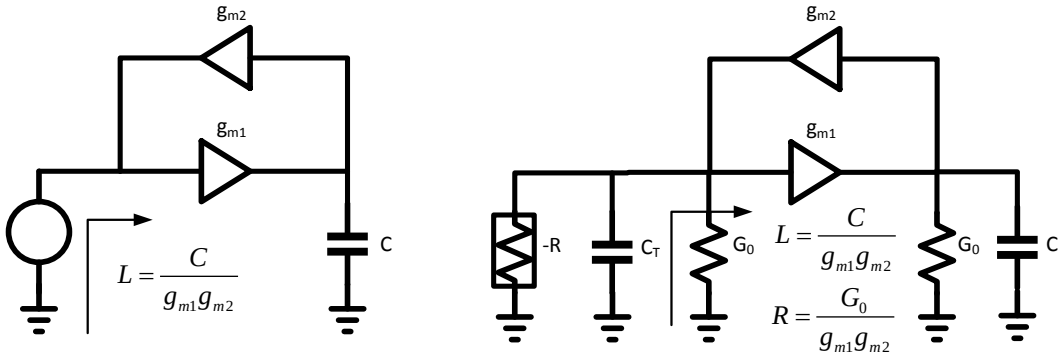

(a) (b)

Figure 4.6 Active inductance and resonator

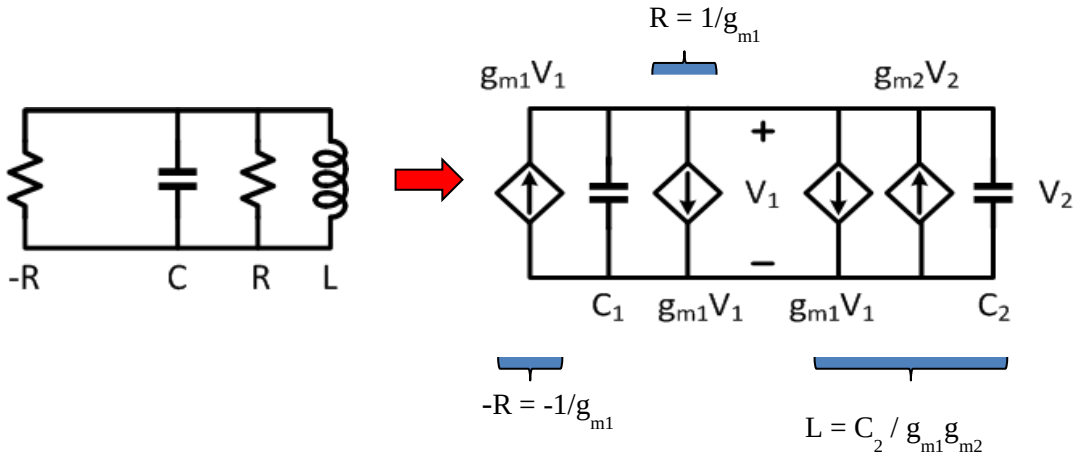

Figure 4.7 Equivalent circuit of the designed inverter based active resonator

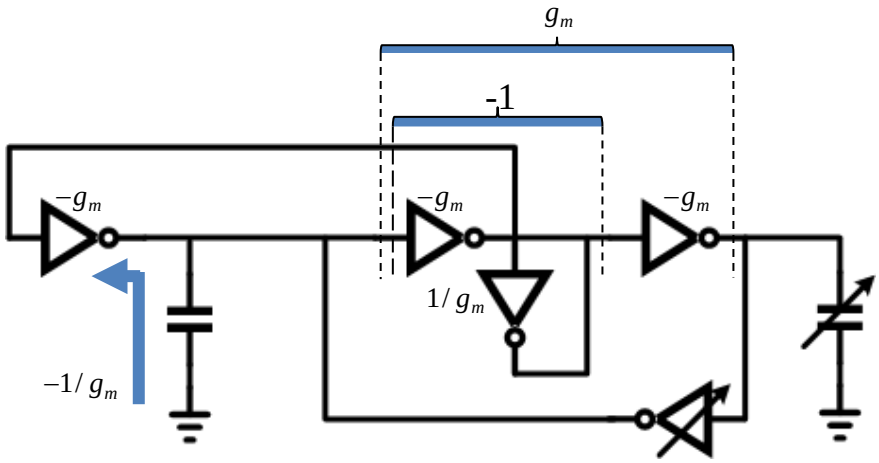

Figure 4.8 Circuit realization of the inverter based active resonator

In order to circumvent the use of an off chip inductor while still maintaining the sinusoidal output and frequency dependency of C in that of a LC tank, active-inductor based oscillator design was proposed. As shown in Fig 4.6.a, an inductive impedance can be achieved by a capacitively loaded gyrator. The equivalent inductance, $C / g_{m1}g_{m2}$, can be easily made in the µH range if C is in the pF range and the two g_m's are in the mS range, which is typical in short channel analog design. By pairing this active inductor

with another capacitor and a negative resistance, an active implementation of a resonator is realized (Fig 4.6.b)

Active resonators are not free of their problems, however. Due to the use of active devices, they are noisier than resonators built from physical inductors and capacitors of the same value. The commonly reported phase noise measurement of active resonators is about 20-30dBc/Hz higher than their passive counterpart. In [18], it is also mentioned that the non-linear characteristics of amplifiers reduces maximum amplitude swing and therefore the dynamic range of active resonator is restricted. For the phase noise problem, since the oscillation frequency is low in the MHz range, and that the oscillator signal is only fed into a counter, the phase noise performance is not as critical as in wireless or wireline communication applications. Nonetheless, as Professor Abidi has proved in [19] that noise of active resonators is proportional to the Q of the tank and has given an expression for the Q, attempt for slight improvement in phase noise was made. Although not many design freedom is left as the component values are dictated by panel construction and frequency of oscillation, the Q of the active resonator was set to a low value (around 2) by setting the ratio between C and C_T. As for the dynamic range problem, a modified version of the design proposed in [20] was adopted. The adopted design replied on the transconductance of CMOS inverters as the Gm stages in the gyrator. Negative impedance in parallel with the tank is also created from inverters to guarantee oscillation. Additionally, a capacitor array is used to supplement C to realize a tunable frequency oscillator (by changing the equivalent inductance). The equivalent circuit and the actual implementation are shown in Fig 4.7 and 4.8. Detailed performance results are presented in Chapter 5.

Chapter 5

System Level Design

5.1 Objectives and Specifications

The aforementioned techniques and circuit designs partially but critically serve the objectives of this work. At a system level, the design must be able to perform singe point (touch or proximity) sensing on a multi-channel PCS panel, which is mostly designed for charge-transfer based sensors at this moment. Since bootstrapping and active resonator are used, the frequency of oscillation should obey the $f = 1/2\pi\sqrt{LC}$ relationship. Taking a step further, the first order detection sensitivity measure used in this work is defined as

$$f_S = \frac{1}{2\pi\sqrt{LC_S}}$$

$$f_D = \frac{1}{2\pi\sqrt{L\left(C_S + C_F\right)}}$$

$$Sensitivity = \frac{f_S - f_D}{f_S} = (1 - \frac{\sqrt{C_S}}{\sqrt{C_S + C_F}}) \times 100\%$$

The definition of isolation is identical to that of sensitivity, except that it is when C_F is applied on non-connected electrodes. The capacitances that bound our design in simulation are

- C_S = 6pF, this value is determined based on the measurement of self-capacitance to ground of a single electrode / channel, which is around 5pF. 1pF was added to cover additional parasitic such as wiring and ESD protection.

- C_F = 100fF, this value complies with literature and is consistent with the amount of capacitance a finger can produce with respect to a touch panel in a distance of 1cm to 2cm.
- C_C = 60pF, the coupling capacitance amongst all electrodes / channels. This value is determined by direct measurement using a precision digital multi-meter.

Based on the above values, the ideal case of sensitivity is $(1-\sqrt{6}/\sqrt{6.1})\times 100\% = 0.823\%$, which is the number system design strives to achieve. Clearly, the sensitivity can see a great improvement when the effective C_S is smaller or a mild improvement with larger C_F. Since the oscillation signal is fed into a counter, the difference in counter result due to modulated frequency is considered as the second-order measure of sensitivity and isolation. However, using counter value requires well-controlled start and stop instant for the integration process, which mandates digital control. As planned, a digital core will be designed when this work proves to be effective. For this reason, first-order frequency measure is the gauge used primarily for simulation of the sensor front end. Counter simulations are presented only to show the health of the design.

As far as multi-channel is concerned, it was decided to design for seven channels with three row electrodes, three column electrodes, and a reference. With such an arrangement, the design will give single detection capability that covers all eight directions, which has the potential for further development (with digital algorithm) for simple gesture recognition.

5.2 Design Considerations for Multi-Channel Detection

Even though the concept prototype shown in Fig 2.4 was designed with a single sensing electrode, it has one additional electrode as the reference, which is designed to be irresponsive to finger touch. The amount of frequency modulation is determined by comparing counter values of the following two scenarios,

1. (Step 1) the oscillator is loaded with the reference electrode and count for some sufficient number of cycles, say 1000, and the first counter value is obtained.
2. (Step 2) As in the Dicke switch configuration, the oscillator is loaded with the sensing electrode. The counter is set to run for another 1000 cycles and a second counter value is obtained.

The ratio of the difference of the two counter values to the reference value is used by digital detection algorithm. One issue remains that if the two loads are intrinsically unequal even without the presence of C_F, erroneous sensing results become probable. This problem extends to design of many channels as each active channel is compared to the reference channel during one scan. A calibration process is therefore required to effectively equalize the load among all channels before detection.

One option to implement such calibration is to rely on digital algorithm. For example, for a two-channel sensor (e.g. one row, one column, and one reference), all the channels are scanned in a controlled environment where none of the channels are loaded with extra capacitance. Their respective counter values, N_1, N_2, and N_0, are obtained. The difference to reference of each channel, $\Delta_1 = N_1 - N_0$ and $\Delta_2 = N_2 - N_0$, are stored in memory. During normal operation, when the row electrode is scanned, Δ_1 is added to the

counter value; when the column electrode is scanned, Δ_2 is added to the counter value. The corrected values are used for detection algorithm instead of the actual readings during the normal operation. Although simple and elegant with no need for extra analog hardware, the digital calibration approach has a fatal disadvantage due to the use of free running oscillator. The oscillation frequency will drift over temperature and over environmental changes. In a more humid day, the reference frequency can be different from that obtained during calibration, which means the store values for correction are no longer valid.

From the drawback of digital calibration, it can be learned that the calibration should be applied to the actual capacitive loading instead of their translations, such as frequency and counter values. Borrowing concept from successive approximation (SAR) used in analog-to-digital converter, a binary capacitor array was added to the design. Using this array, the calibration process can be explained again using the two-channel sensor example,

1. In a controlled environment, scan through all channels and record respective counter value.
2. For example, the row electrode, E_1 has the smallest counter value, N_1, and therefore the largest path loading. E_1 is considered as the reference for calibration.
3. When E_0, the reference electrode, is connected to load the oscillator, the capacitor array is also connected as if they are part of the reference electrode loading. A SAR-like control is applied to the array starting with the code for the largest capacitance value. The counter is then enabled and a value is obtained. If the reading is less than N_1, the code for half the total capacitance is applied.

Oscillation starts again and the resulting counter value is once again compared to N1 and subsequent control code ensues. This process continues until all control bits are covered and is repeated for E_2.

4. The final control bits are stored in the digital core memory. During normal operation, whenever a channel is scanned, the corresponding control bits are applied to the switches for the capacitor array to keep the loading from each other approximately equal.

The specification of the calibration capacitor array is naturally its range and resolution. The range is set to 1.5pF, which goes under the assumption that if any path difference exceeds this value, one of the paths is not well designed. The resolution is set to 25fF, which means any two channel loadings will be within 25fF of difference. Such value is determined so that it is a fraction of C_F and it is not so small as to prolong calibration time. The array in the final design covers 1MHz range in terms of frequency and achieves a frequency resolution of 0.01MHz.

5.3 Frequency Tuning of the Oscillator

Serving the purpose of a test chip, the design must have tunable variables for debug and optimization. The most critical variable in this design is the frequency of oscillation, which not only puts a requirement on the bandwidth of bootstrapping amplifier but also affects the number of cycles available for integration. The frequency of the oscillator in this design is made tunable by changing the active inductance, $L = C / g_{m1} g_{m2}$ with a digital controlled capacitor array for adjusting the gyrator-loading

capacitor C. Due to the bandwidth limit of the designed OTA, the frequency covers one octave of range from around 3MHz to 6MHz in 16 steps.

5.4 Switch Design

Multi-channel design and the use of capacitor arrays ask for many switches. As the oscillation signal itself is centered around mid-VDD, the switches take the form of transmission gates. For the calibration capacitor array and tuning capacitor array, the switches are sized relatively small so that their parasitic capacitance does not overwhelm the array unit capacitor. The channel switches, on the other hand, requires a different strategy, as the loading capacitance is fairly large comparing to device parasitic.

During early testing of the concept prototype, the chip showed vulnerability to ESD damage even though ESD protection was included in the pad design and protective wristband was used during testing. Re-doing the design in this work, it is found that the only path that pad ESD protection could not protect is from the panel and through the channel switch, where the switch transistors take direct damage. For better ESD protection, thick oxide devices are used for channel switches. Since thick oxide devices run on a 2.5V supply, the oscillation signal only requires zero passing – only NMOS switches are needed and they can be sized larger as the PMOS parasitic no longer exists. The larger size of the switches in this case brings two distinct benefits. The on-off resistance ratio increases with larger switch size, which in turn improves the isolation as defined at the beginning of this chapter. The smaller on-resistance also compensates for the parasitic resistance of the ITO trace on the touch panel. The smaller the path resistance, the more effective capacitance is seen by the oscillator as the capacitor-

resistor network has a higher Q value. The use of thick oxide devices requires level shifters for translating 1V control signal to be applied to the switches. The 2.5V VDD is tapped off from the ESD protection pad.

5.5 System Integration and Selected Simulations

Incorporating every component discussed so far and adding necessary connections and logic, the scope of the AFE is defined, which includes

1. Seven channels, that is, three row electrodes, three column electrodes, and one reference electrode, covering all eight directions in the XY plane
2. Inverter based active resonator with capacitor array for frequency tuning
3. OTA for bootstrapping
4. Calibration capacitor array for equalizing loading of channels
5. 3-to-8 decoder for channel selection
6. Level shifters for driving the thick oxide switches connecting the sensor circuitry and the panel
7. 16-bit counter
8. UART for communication between the counter and PC
9. Analog I/O’s for oscillator frequency tuning, calibration (done manually in this design), channel selection, and output monitoring.

The entire system is shown schematically in Fig 5.1. Note that the oscillator output is fed into three different places, analog pad, digital pad, and the counter. This configuration adds more debug capability to the system.

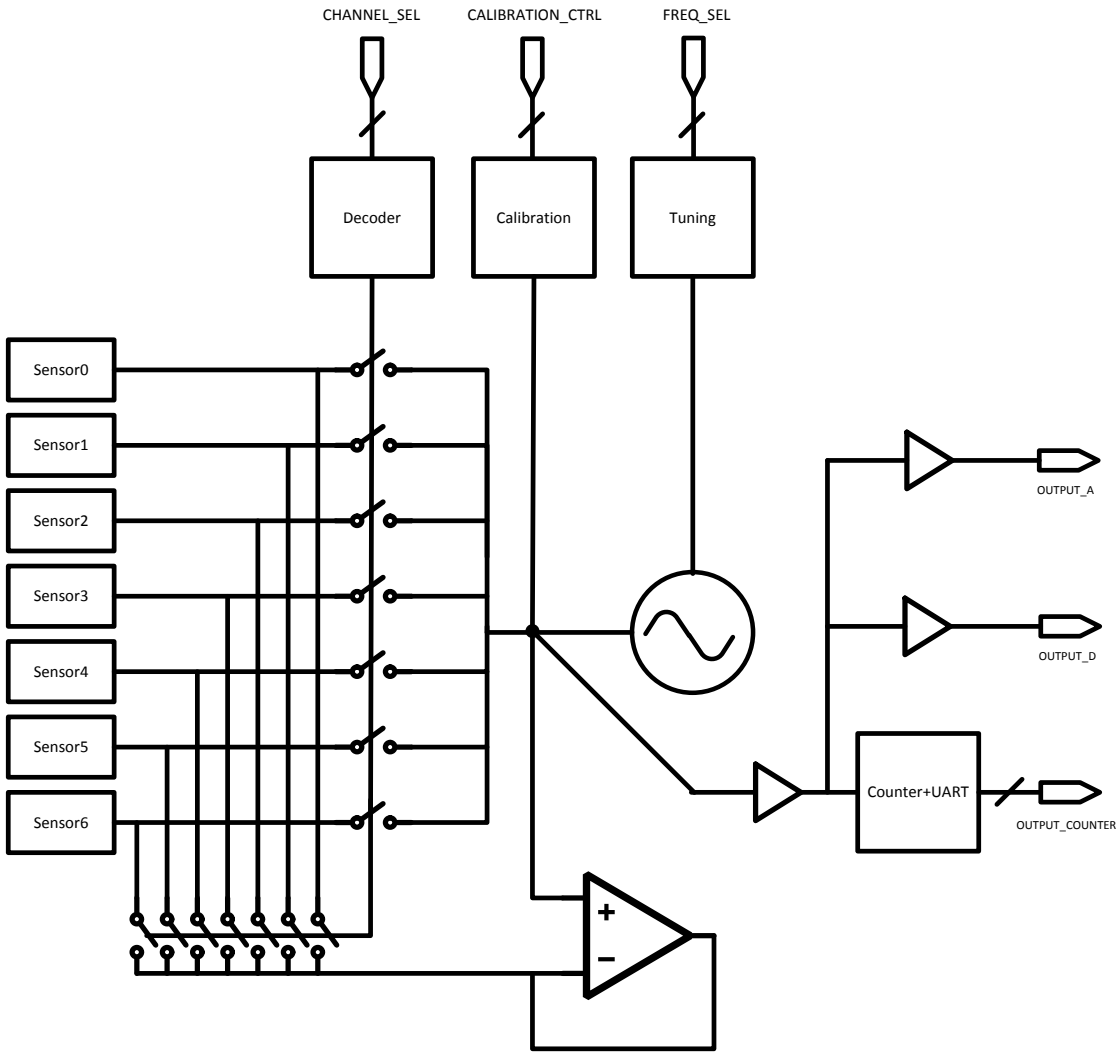

Figure 5.1 System level diagram of the sensor front end and readout circuit

Simulations at both the block level and the system level are performed to verify the design. Fig 5.2 – 5.4 shows the oscillator performance. Fig 5.5 and Table 5.1 summarize the performance of the OTA. In order to check the robustness of the design, each block is verified at 135 PVT corners.

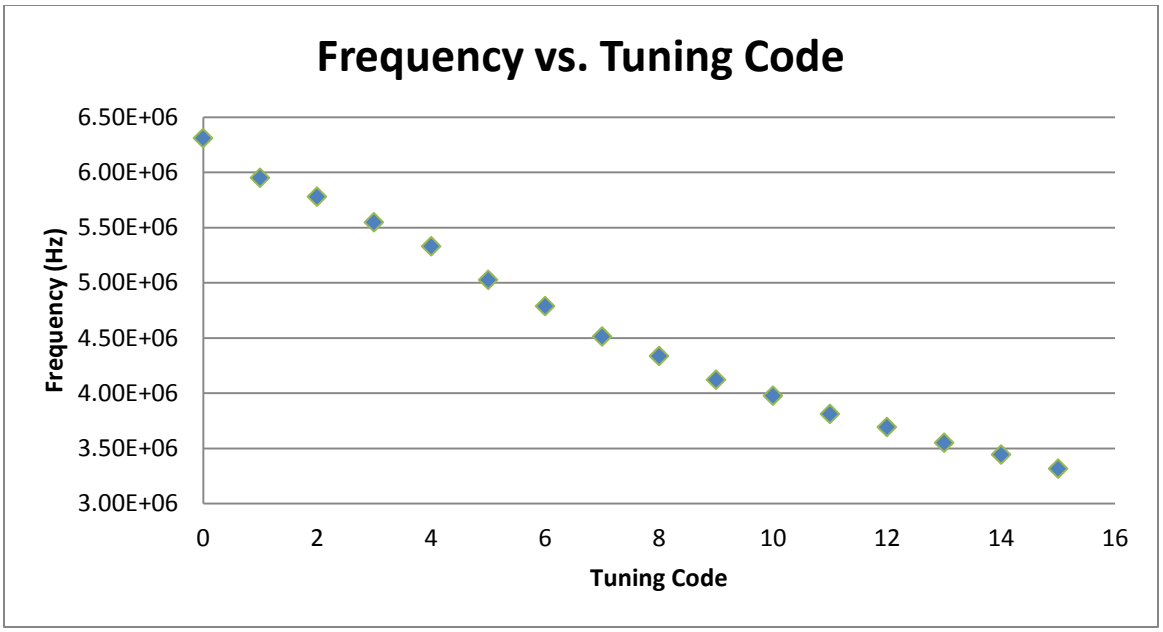

Figure 5.2 Varying oscillator frequency with different tuning capacitor array values

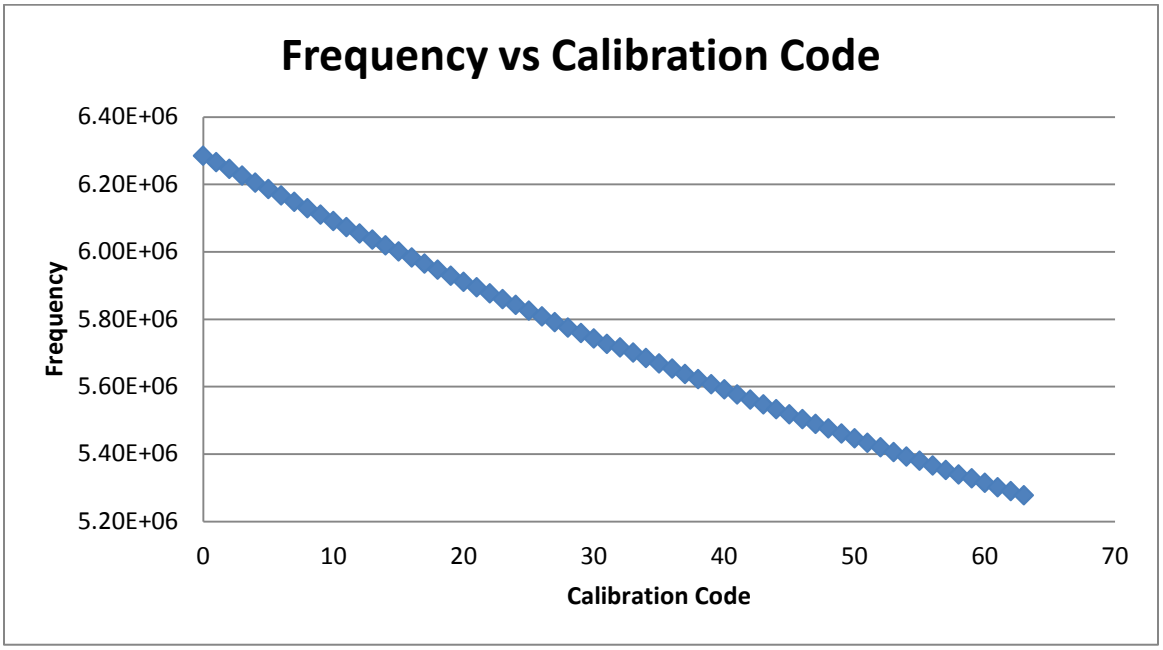

Figure 5.3 Varying oscillator frequency with different calibration capacitor array values

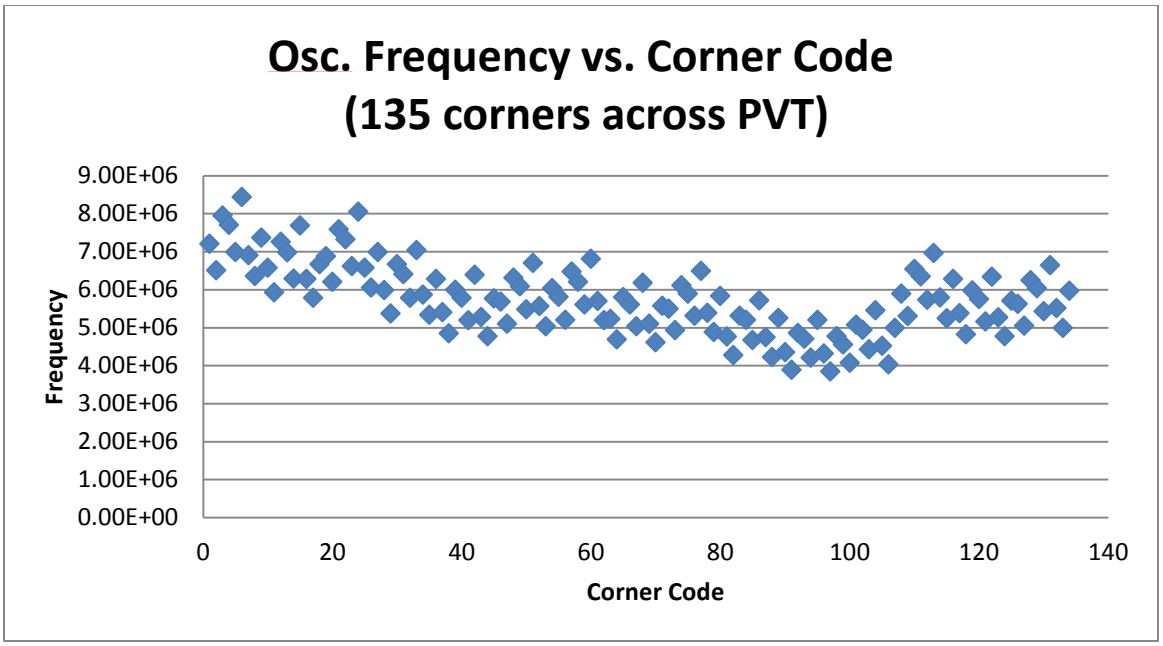

Figure 5.4 Oscillator frequency against PVT variation

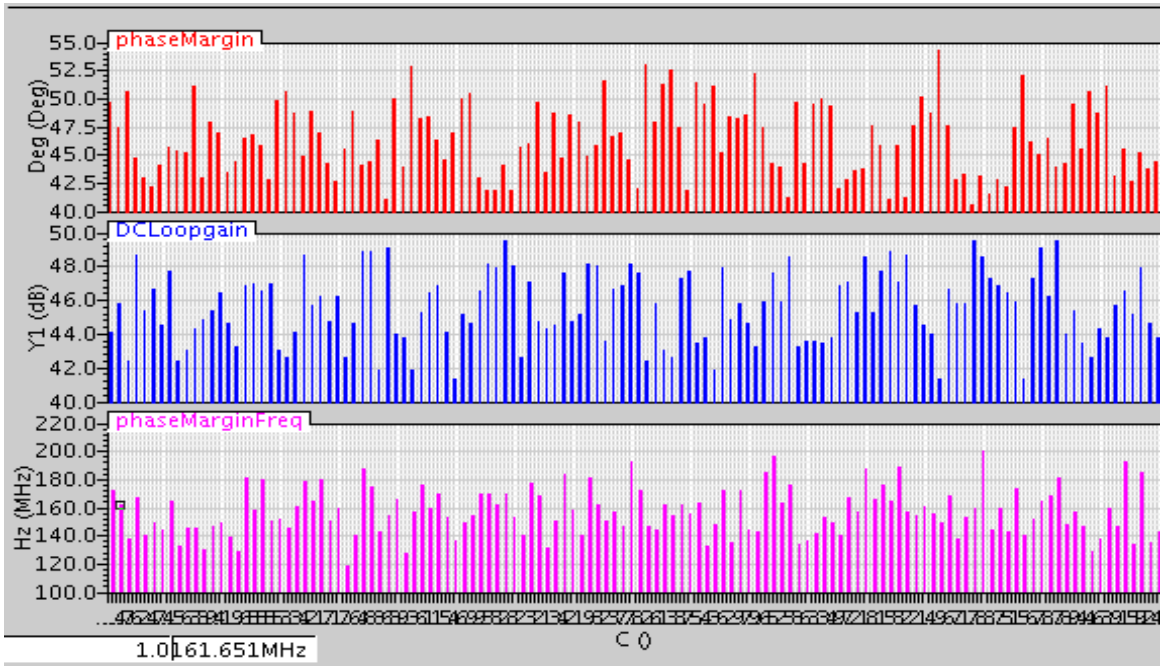

Figure 5.5 OTA DC gain and phase margin across PVT corners

1V, 50degree Cc=60pF Cload=20pF	Prelayout		Postlayout	
	DC Gain	Phase Margin	DC Gain	Phase Margin
ttt corner	46.09dB	50.3	45.64dB	47.61
fft corner	45.70dB	50.25	45.24dB	47.53
sst corner	46.25dB	50.45	45.81dB	47.83

Table 5.1 summary of OTA performance

At the system level, the test bench is set up with the panel modeled as in Fig 3.5 with one of channels has extract capacitance due to C_F. Transient simulation is applied to mimic real usage case. In Fig 5.6, the switch signal first remains low, indicating that no C_F is added. At 40µs, the switch signal goes high, connecting the channel with C_F, and consequently causing the oscillation frequency to drop from 4.661MHz to 4.628MHz. The sensitivity is calculated to be 0.71% in this case.

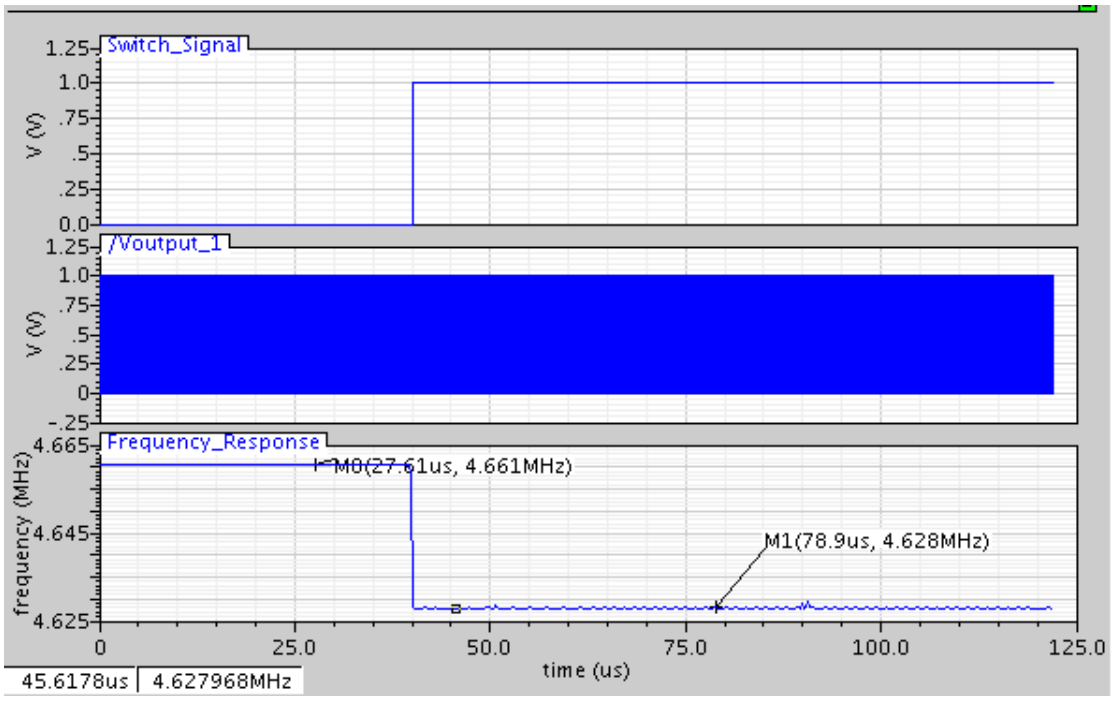

Figure 5.6 Transient simulation of C_F induced frequency change

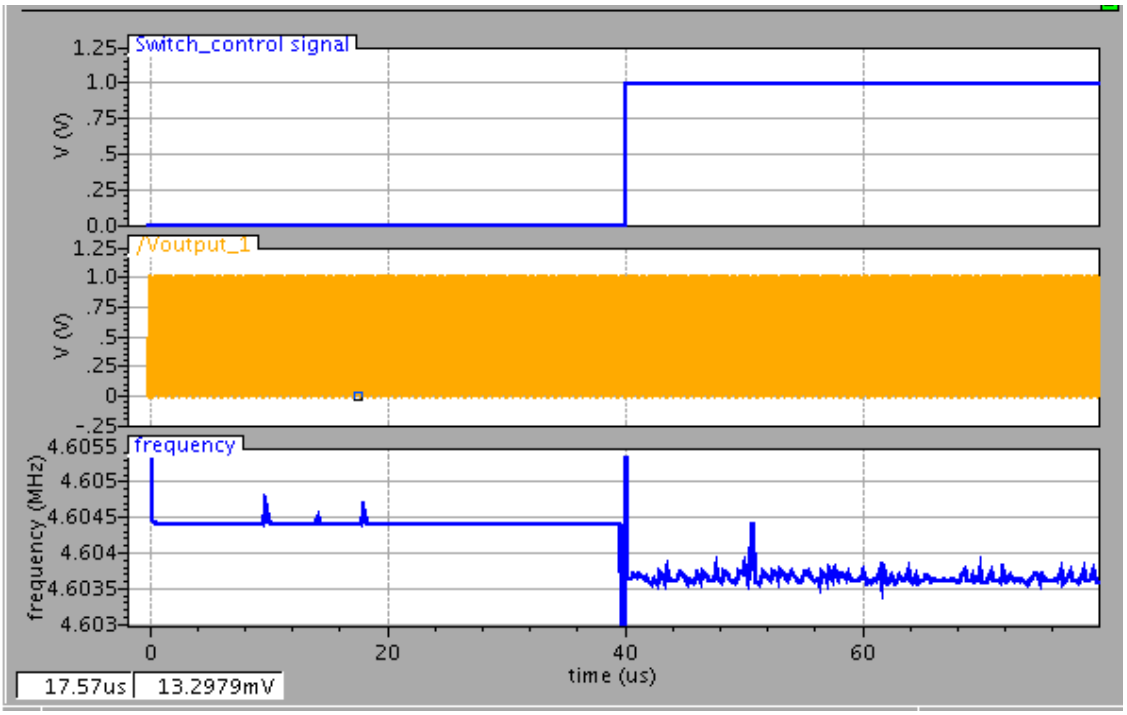

Figure 5.7 Transient simulation of C_F induced frequency change from non-connected channel

Applying the same strategy, the isolation can be measured. In this case, when the switch signal goes high at 40µs, a regular channel without C_F is connected. Due to non-ideal bootstrapping and non-ideal switching, some coupling from C_F can still be seen and this causes a frequency change from 4.6044MHz to 4.6037MHz, yielding an isolation of 0.015%, which is almost 50 times smaller than the sensitivity measure based on Fig 5.7.

System level simulation was also tested with different frequencies (tuned via the capacitor array) and across PVTs. In general, it is observed that at lower frequencies, sensitivity is better, which is reasonable because bootstrapping is closer to ideal with the OTA running at lower frequency with higher gain. Table 5.2 shows the simulation result at different corners with different tuning capacitor settings (controlled by Vcfg). Due to the long simulation time for mixed-signal simulation in Cadence, the results are prelayout.

Corner	fft 27	fft_100	sst_27	sst_100	ttt_27	ttt_100
Load change from 6p to 6.1p	Vcfg=3	Vcfg=7	Vcfg=3	Vcfg=7	Vcfg=3	Vcfg=7
Frequency at 6p (MHz)	7.01	5.47	4.89	3.87	5.88	4.65
Frequency at 6.1p (MHz)	6.94	5.43	4.84	3.85	5.83	4.61
Counter value at 6p (x1000)	2.15	1.94	1.70	1.16	1.87	1.40
Counter value at 6.1p (x1000)	2.13	1.90	1.69	1.15	1.84	1.39
Sensitivity in frequency (%)	0.956	0.713	0.982	0.723	0.952	0.731

Table 5.2 Summary of sensitivity of the system (pre-layout)

As mentioned, the use of digital counter values for sensitivity measure requires careful control in order to eliminate errors caused by the oscillator stabilization process after each switching activity. Such a control algorithm is not implemented in the form of digital logic for the AFE and thus counter value is not used for sensitivity calculation in Table 5.2. The health of the digital counter and UART is nonetheless critical because the control algorithm can still be applied manually during testing and there is potential for FPGA integration when the control algorithm is implemented in FPGA.

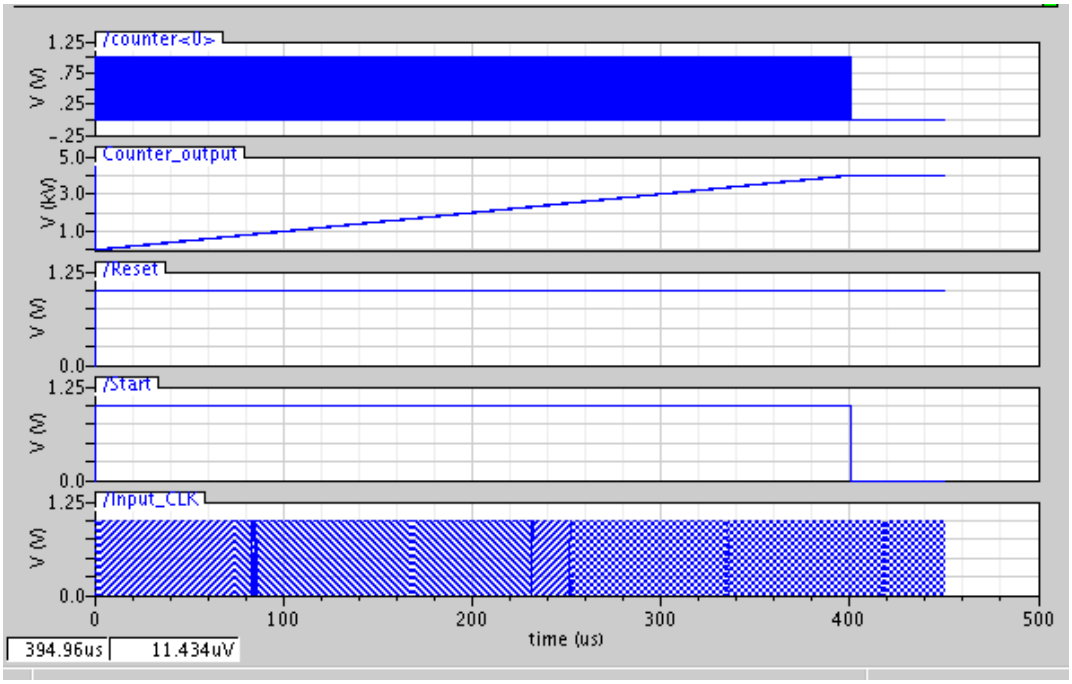

Figure 5.8 Transient simulations of the counter and UART

Fig 5.8 shows the post layout simulation of the digital counter with UART control. It can be seen that counter is incrementing with constant input clock signal. The counter_output signal in Fig 5.8 is after binary-to-decimal conversion through an ideal DAC and hence the observed staircase-like incrementing pattern.

The total power consumption of the design is simulated to be about 6mW, which is significantly smaller than the 20mW reported in [16] and the conventional charg-transfer based designs such as [14]. The OTA takes the majority at 4mW while the output buffer takes 1.2mW. The oscillator only consumes 0.2mW of power and the digital block 0.5mW. Fig 5.9 shows the chip layout. The design has been submitted to TSMC for fabrication.

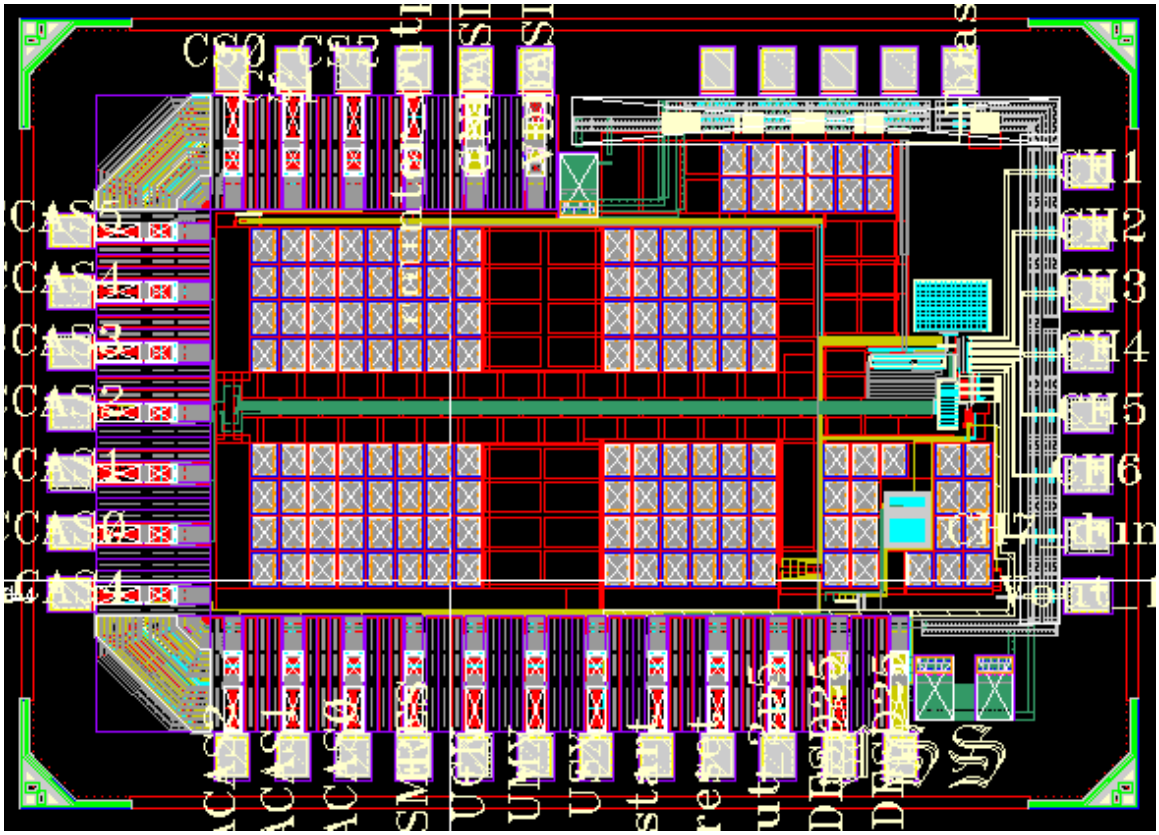

Figure 5.9 Chip layout

Chapter 6

Conclusion and Future Work

6.1 Conclusion to This Work

An oscillator-based capacitive sensing analog front end is developed for the existing PCS touch panel targeting applications such as phones, tablets, and PCs. The design accentuates 3D detection capability by the application of the following techniques

1. The use of reference electrode for comparison through a Dicke switch configuration for low frequency environmental fluctuation
2. High frequency oscillation driving counter to integrate the effect of random noise
3. Op-amp bootstrapping for minimizing both channel-to-channel coupling and finger cap fringing

This work started with the testing and characterization of an earlier concept prototype in Fig 2.4. From the debugging process, as well as the interaction with touch panel vendors, better understanding about the prevailing PCS technology and about the touch panel was consolidated. Such understanding helped explained several drawbacks of the concept prototype and eventually led to the re-design presented here. The design presented here started with modeling with ideal components in simulation, preceded then to prototyping with off-the-shelf components, then schematic entry and layout, and finally integration of the entire chip. Due to inconvenient tape-out schedule of the MPW program, the design has not made it back to the lab from the foundry. The results presented here are based on post layout simulations unless denoted otherwise.

6.2 Future Improvement and Research Direction

Time was limited when working on this project and one of the main causes was that the problem definition had to be drawn out from debugging. Once the problem was defined, focus was given to find a viable solution and to make it work. The project, unlike a conventional circuit design problem, incorporates both analog and digital designs and is effectively a miniature SoC. So much effort was put into making everything working together with some degree of robustness but not so much into optimization.

At the circuit level, although the oscillator has robust rail-to-rail swing, the simply designed OTA, however, does not take rail-to-rail input. The current solution is to clamp every inverter swing in the active resonator using two diodes so that the oscillator swing is acceptable to the op-amp. It is a simple and effective technique yet process variation tends to affect the swing. Great amount of PVT simulations were performed to make sure that the amplitude does not go to zero under extreme corner cases. A more artistic yet time consuming approach is to either modify the active resonator design or the op-amp design. The op-amp, which drives a large capacitor with some serial resistance, should ideally be designed with a proper output stage. To the extreme, an op-amp with GHz bandwidth, rail-to-rail input, and the ability to drive arbitrary load would be ideal and should even be power optimized. Driven by the love for analog design, such challenges attract me yet it is also reasonable to apply such optimization once the bootstrap idea is fully demonstrated.

Probably the one thing that is interesting to add to this work had more time been available is the modeling of all noises sources in the sensor environment and to see

whether or how the techniques applied can improve the SNR. To this point, the concept of SNR in the context of touch sensing has not been introduced. Such omission was intentional as the SNR is more applicable during testing if noises are not probably modeled in simulation. An official definition of SNR is given in [11]

$$SNR(dB) = 20\log(TouchStrength / NoiseTouched_{RMS100})$$

$$TouchStrength = SignalTouched_{AVG100} - SignalUntouched_{AVG100}$$

$$NoiseTouched_{RMS100} = \sqrt{\frac{\sum_{n=0}^{n=99}(Signal[n] - SignalTouched_{AVG100})^2}{100}}$$

where:

- AVG100 means the simple numeric average of 100 data points, typically taken evenly spaced over a period of 2 seconds.
- RMS100 means the root-mean-square of 100 data points, typically taken evenly spaced over a period of 2 seconds, using the AVG100 figure as a baseline.

For charge-transfer based sensing techniques, signal is the voltage level converted from charging the mutual capacitance. For oscillator-based sensing techniques, signal is basically the frequency of oscillation. Since most noise sources exhibits charge or voltage characteristics in a highly capacitive environment of PCS panels, the noise adds directly to the signal level. When oscillator-based sensing techniques are applied, the relationship or translation from voltage or charge noise to frequency perturbation may be somewhat intricate. One concrete example is the 50/60Hz AC coupling noise from the panel. Such noise directly adds to the charge-to-voltage output voltage as voltage measurement is

probed right off the panel. On the other hand, such noise presents itself at the load of an oscillator with specific spectrum characteristics. The outcome is yet to be investigated. Modelling all the noise sources is a must-do in the future if it comes down to maximizing SNR comparing to conventional sensing method.

During the gap period until the die is shipped back from the foundry, compatible PCB will be designed and a more controlled testing apparatus will be set up. Digital core will also be implemented. Once the design proves working, the natural next step is to extend the design to cover more channels as a complete system with digital core integrated. As mentioned in Chapter 2, current design serves only single point sensing – a feature with diminishing market. It is still a mystery as for the limitations of the conventional mutual capacitance sensing when it is applied to 3D detection. True breakthrough lies in the full analysis of such limitations and overcoming them to realize a high resolution multi-touch 3D sensor.

Reference

[1] Hyunsoo Ha; Sylvester, D.; Blaauw, D.; Jae-Yoon Sim, "12.6 A 160nW 63.9fJ/conversion-step capacitance-to-digital converter for ultra-low-power wireless sensor nodes," Solid-State Circuits Conference Digest of Technical Papers (ISSCC), 2014 IEEE International , vol., no., pp.220,221, 9-13 Feb. 2014

[2] Przybyla, R.J.; Hao-Yen Tang; Shelton, S.E.; Horsley, D.A.; Boser, B.E., "12.1 3D ultrasonic gesture recognition," Solid-State Circuits Conference Digest of Technical Papers (ISSCC), 2014 IEEE International , vol., no., pp.210,211, 9-13 Feb. 2014

[3] Hamaguchi, M.; Nagao, A.; Miyamoto, M., "12.3 A 240Hz-reporting-rate 143×81 mutual-capacitance touch-sensing analog front-end IC with 37dB SNR for 1mm-diameter stylus," Solid-State Circuits Conference Digest of Technical Papers (ISSCC), 2014 IEEE International , vol., no., pp.214,215, 9-13 Feb. 2014

[4] Du, Li. (2013). Oscillator-Based Touch Sensor with Adaptive Resolution. UCLA: Electrical Engineering 0303. Retrieved from: http://escholarship.org/uc/item/0t2982ft

[5] http://www.dmccoltd.com/english/museum/touchscreens/

[6] http://en.wikipedia.org/wiki/Theremin

[7] Barrett, G. and Omote, R. Projected-Capacitive Touch Technology. Information Display. (26) 3, 20 16--21.

[8] Madaan, Pushek, and Priyadeep Kaur. "An Introduction to Capacitive Sensing-Part I | EE Times." EETimes. Cypress Semiconductor, 16 Apr. 2012.

[9] Lasanen, K.; Kostamovaara, J., "A 1.2-V CMOS RC Oscillator for Capacitive and Resistive Sensor Applications," Instrumentation and Measurement, IEEE Transactions on , vol.57, no.12, pp.2792,2800, Dec. 2008

[10] O'Dowd, J.; Callanan, A.; Banarie, G.; Company-Bosch, E., "Capacitive sensor interfacing using sigma-delta techniques," Sensors, 2005 IEEE , vol., no., pp.4 pp.,, Oct. 30 2005-Nov. 3 2005

[11] ATMEL Corporation, “Touch Sensors Design Guide, 10620D-AT42” Sept. 2004

[12] Miura, N.; Dosho, S.; Takaya, S.; Fujimoto, D.; Kiriyama, T.; Tezuka, H.; Miki, T.; Yanagawa, H.; Nagata, M., "12.4 A 1mm-pitch 80×80-channel 322Hz-frame-rate touch sensor with two-step dual-mode capacitance scan," Solid-State Circuits Conference Digest of Technical Papers (ISSCC), 2014 IEEE International , vol., no., pp.216,217, 9-13 Feb. 2014

[13] http://en.wikipedia.org/wiki/Multi-touch

[14] Seunghoon Ko; Hyungcheol Shin; Jaemin Lee; Hongjae Jang; Byeong-Cheol So; Ilhyun Yun; Kwyro Lee, "Low noise capacitive sensor for multi-touch mobile handset's applications," Solid State Circuits Conference (A-SSCC), 2010 IEEE Asian , vol., no., pp.1,4, 8-10 Nov. 2010

[15] Sansen, Willy M. C. "Differential Voltage and Current Amplifiers." Analog Design Essentials. Dordrecht: Springer, 2006. 89-115.

[16] Yingzhe Hu; Liechao Huang; Rieutort-Louis, W.; Sanz-Robinson, J.; Wagner, S.; Sturm, J.C.; Verma, N., "12.2 3D gesture-sensing system for interactive displays based on extended-range capacitive sensing," Solid-State Circuits Conference Digest of Technical Papers (ISSCC), 2014 IEEE International , vol., no., pp.212,213, 9-13 Feb. 2014

[17] Lee, T.H.; Hajimiri, A., "Oscillator phase noise: a tutorial," Solid-State Circuits, IEEE Journal of , vol.35, no.3, pp.326,336, March 2000

[18] Szczepkowski, Grzegorz; Farrell, Ronan, "Analysis and design of oscillators based on low-voltage self-oscillating active inductors," Signals and Systems Conference (ISSC 2010), IET Irish , vol., no., pp.135,140, 23-24 June 2010

[19] Abidi, A.A., "Noise in active resonators and the available dynamic range," Circuits and Systems I: Fundamental Theory and Applications, IEEE Transactions on , vol.39, no.4, pp.296,299, Apr 1992

[20] Barthelemy, H.; Bourdel, S.; Gaubert, J.; Battista, M., "CMOS inverters based high frequency voltage controlled sinusoidal oscillator," Electronics, Circuits and Systems, 2007. ICECS 2007. 14th IEEE International Conference on , vol., no., pp.490,493, 11-14 Dec. 2007